Bacteria-triggered Release of a Potent Biocide from Core-shell Polyhydroxyalkanoate (PHA)-based Nanofibers for Wound Dressing Application

by

Wei Li

A Thesis submitted to the Faculty of Graduate Studies of

The University of Manitoba

in partial fulfilment of the requirements of the degree of

Master of Science

Department of Biosystems Engineering

University of Manitoba

Winnipeg

Abstract

Bacterial infection is a serious issue in wound healing. Extensive use of biocides in wound dressings have raised concerns like biocide resistance and unwanted harm to normal skin cells. In this thesis, I report a new approach to realize bacteria-triggered release of biocide to the sites of bacterial infections from core-shell polyhydroxyalkanoate (PHA)-based nanofibers prepared by coaxial electrospinning. The hydrophobic PHA-based shell can effectively prevent the biocide from undesirable payload release in physiological environments without pathogens. However, in the presence of pathogens, the PHA-based shell is degraded by pathogens, and the encapsulated biocide is released. The released biocide subsequently can impose targeted antimicrobial effects on the bacteria. Using *Pseudomonas aeruginosa* as a model bacterium and dodecyltrimethylammonium chloride as a model biocide, we demonstrated that the core-shell PHA-based nanofibers released encapsulated dodecyltrimethylammonium chloride in the presence of *Pseudomonas aeruginosa*, resulting in targeted inhibition of *Pseudomonas aeruginosa* growth.

Acknowledgement

Undertaking this master degree has been a challenging experience for me and I could not make it without the support and help received from many people. I would like to express my gratitude to my supervisor, Dr. Song Liu, for his support, guidance, and help during my M.Sc. program. I appreciate his vast knowledge, ideas, and encouragement to make my research experience motivational, productive, and enjoyable. It has been a great honour to work and learn from him. Thanks to his efforts, I have grown tremendously in both my academic and personal life.

A special thanks goes to my co-advisor, Dr. Nazim Cicek, without whose financial support and encouragement I may not fully focus on my research program during my two-year M.Sc. program. I must also thank Dr. David B. Levin for all the guidance and assistance throughout my graduate studies. It has been such a valuable experience for me to cooperate with different students in Dr. Levin's group. I am also greatly thankful to Dr. Sarvesh Logsetty for his valuable comments in my committee meetings.

I also want to thank all my friends who helped me get through my M.Sc. program. Some friends, like Seungil Kim and Dr. Hardev Singh, were kind and tolerant enough to teach me chemistry laboratory technique and professionalism. Sadegh Ghanbar, Zahra Abdali, Mohammad Reza Kazemian, Jie Li, and Lucy Wang, were good enough not to throw me overboard while at sea. And I would like to send my thanks out to Dr. Levin's PhD students Christopher Dartiailh and Warren Blunt, for their help in all aspects of our collaboration.

I thank with love to my wife, Xing Xie, for her continuous support, understanding, and encouragement. She has made countless sacrifices to help me get to this point. This thesis has been written during my stay at the Department of Biosystems Engineering of the University of Manitoba. I would like to thank the University of Manitoba Faculty of Graduate Studies for providing me excellent study environment.

Table of Contents

List of Tables

List of Figures

1. Introduction

1.1. Overview

At some stage in life most people have experienced a wound. Wound healing is usually a simple and rapid process. However, for those suffering from diseases such as diabetes, obesity, and cancer, wound healing may be delayed, which may increase susceptibility to bacterial colonization at the wound site and deteriorate the patients' quality of life [1]. Chronic wounds such as ulcers are often heavily contaminated with microorganisms and usually involve significant tissue loss that can cause life-threatening illness.

Wound dressings are designed to shield a wound from contamination. The usual passive dressings such as gauze and tulle, act as a wound cover to help reduce the risk of infection, stop bleeding, and absorb any excess exudate. But these dressings cannot kill bacteria on the wound sites. A functionalized wound dressing incorporated with biocides can play an active role in the wound healing process by preventing or treating infection. However, anti-bacterial treatment of wounds with biocides raises other concerns such as biocide resistance and cross-resistance between biocides and antibiotics. Typical broad-spectrum potent biocides could attack pathogens and host cells non-selectively, further delaying wound healing. Since controlled antibacterial delivery from wound dressings has not been perfected [2], this research intends to develop a wound dressing having an innovative on-demand release of biocides or antibacterial agents triggered by bacterial strains on wound sites.

An important feature in the development of this wound dressing is the manufacture of polymeric nanofibrous mats made of ultra-fine fibers. The high surface area to volume ratio and micro-porosity of these nanofibers make them suited for wound dressings. In addition, nanofibrous morphology has shown improved interactions with cells, like guidance and orientation of regenerating cells and their processes [3].

Electrospinning is a simple and cost-effective way to fabricate nanofibers with a diameter ranging from 7-5000 nm [4]. By applying a high voltage to the polymer solution, nanofibers are formed as the solution or melt is drawn from the nozzle toward a collector. After a certain time, polymeric nanofibrous mats can be collected. For wound care applications, biocides can be easily incorporated into the carrier polymers. Recently, coaxial electrospinning is usually used to fabricate core-shell fibers, consist of a polymeric shell and a core containing biocides. With this method, burst release of biocides in the initial stage can be greatly inhibited, and a sustained efficacy is achieved.

A variety of natural and synthetic polymers have been successfully electrospun into micro/nano structures used for tissue engineering, regenerative medicine and scaffolds [5-9]. Biodegradable and biocompatible polymers attract more and more attention since they do not produce toxins or harmful products and under biological conditions they degrade into by-products which are eventually reabsorbed or reused in nature [10]. Among these biodegradable polymers, polyhydroxyalkanoates (PHAs) (Fig. 1-1) are promising materials for biomedical applications[9].

PHAs are a class of naturally occurring polyesters of various hydroxycarboxylic acids, which are produced and accumulated by many organisms in the form of intracellular granules to store carbon and energy when they are subjected to conditions of lack of nutrients [11]. Two main types of PHAs are generally distinguished, namely short-chain length PHAs (scl-PHAs), consisting of 4-5 carbon atoms per repetition unit, and medium-chain length PHAs (mcl-PHAs), with 6-14 carbon atoms per repetition unit [12]. Compared to the most extensively investigated biodegradable and biocompatible polyesters such as polylactic acid (PLA) [13], polyglycolic acid (PGA) [14], poly(caprolactone) (PCL) [15] and poly(lactic-co-glycolic) (PLGA) [16], PHAs are superior for the following reasons. By tuning the monomer composition, PHA polymers with desired properties can be developed; in contrast, the monomer compositions of PLA, PGA, PCL or PLGA are difficult

to change. PHAs are biopolymers that are produced completely through a biological process: no industrial pollution is produced. The monomers of PHA degradation are less acidic than those of PLA, PGA and PLGA [17, 18]. Large amounts of acidic monomers might overwhelm the human body's capacity to provide adequate local buffering, and could be detrimental to surrounding cells and tissue [19]. Lactic acid and glycolic acid have pKa values of 3.86 and 3.6 respectively, while butyric acid has a pKa value of 4.82. Other PHAs monomers, such as valeric acid and hexanoic acid, have higher pKa values of 4.84 and 4.88. Hence PHAs are more suitable candidates for wound dressings.

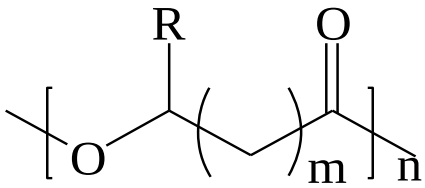

Fig. 1-1. Generic chemical structure of PHA.

Lipases, or extracellular enzymes [20], can be produced and secreted by bacteria and are abundant at sites of wound infections [21]. As early as 1901, *Bacillus prodigiosus*, *B. pyocyaneus*, and *B. fluorescens* were observed to release lipase enzymes. Some of today's best studied lipase-producing bacteria are *Serratia marcescens*, *Pseudomonas fluorescense* and *Pseudomonas aeruginosa* [20].

A unique PHA based core-shell structural nanofibrous mat having a broad-spectrum potent biocide in the core of the nanofibers will be fabricated by coaxial electrospinning. It is hypothesized that the lipases secreted by the most common organisms associated with wound infections (such as *Pseudomonas aeruginosa*) could cleave the ester bonds of the shell polymer. The broad-spectrum potent biocide in the core of nanofibers could then be released to kill the bacteria at the wound site.

1.2. Thesis Objectives

The following are the objectives of this research:

(1) Optimize the fabrication of mcl-PHA nanofibrous mats using an electrospinning technique;

(2) Comprehensively investigate PHA electrospun nanofibrous mats, with a focus on physical and chemical properties and morphology of the nanofibers, and mechanical characterization of the mats;

(3) Design a unique core-shell structural nanofibrous mat using coaxial electrospinning. That method will make the PHA based shell for structural integrity and a broad-spectrum potent biocide in the core of the fiber;

(4) Conduct an *in vitro* release study in phosphate-buffered saline (PBS) solution and cell-free culture supernatant to demonstrate the lipase responsiveness of the unique core-shell nanofibrous mat. The antimicrobial activity of this mat will be quantitatively evaluated by a shake flask test using *Pseudomonas aeruginosa* as the model bacteria.

1.3. Thesis Organization

The body of this thesis is organized into 5 chapters. Chapter 1 is the introduction and design framework of the entire research project. Chapter 2 is a background literature review of the topics of PHA biological properties, electrospinning, PHA electrospinning and its application in the biomedical application field. Chapter 3 covers fabrication of PHA nanofibrous mats using an electrospinning technique, and a comprehensive investigation of PHA electrospun mats with a focus on nanofiber morphology, physical, chemical, and mechanical properties. Chapter 4 discusses the preparation of the core-shell structural nanofibrous mat using coaxial electrospinning. That method makes PHA based shell for structural integrity, and a broad-spectrum biocide in the core of nanofibers. An *in vitro* release study demonstrates that the unique core-shell nanofibrous mat is lipase responsive. The antimicrobial property of this coaxial electrospun mat will be evaluated for wound dressing applications. Chapter 5 discusses the future work and recommendation of the project.

2. Literature Review

2.1. Introduction of a Bioplastic: Polyhydroxyalkanoate

Recently, bioplastics have developed rapidly owing to the environmental pollution related to products made from crude oil. Polyhydroxyalkanoates (PHAs), a class of biopolyesters with diverse monomer structures, are the only bioplastics that can be completely synthesized by microorganisms. In 1926, Lemoigne first discovered polyhydroxybutyrate (PHB) in *Bacillus megaterium* [22]. Since that time, many PHA monomer structures have been reported [23, 24]. Today, nearly 300 different microorganisms have been reported that synthesize PHA under the conditions of nutrient deficiency (nitrogen, phosphate, sulphur, potassium, tin, iron, magnesium or oxygen) [25]. Two main types of PHAs are generally distinguished: short-chain length PHAs (scl-PHAs), consisting of 4-5 carbon atoms per repetition unit, for example poly(3-hydroxybutyrate) (PHB) and poly(3-hydroxybutyrate-co-3-hydroxyvalerate) (PHBV) (Fig. 2-1); and medium-chain length PHAs (mcl-PHAs), having 6-14 carbon atoms per repetition unit [12], for example poly(3-hydroxyoctanoate) P(3HO) and poly (3-hydroxyoctanoate-co-3-hydroxyhexanoate) (PHOHHx) (Fig. 2-2).

In terms of the physical properties, mcl-PHAs have a melting temperature (Tm) in the range of 40 to 60°C, and glass transition temperature (Tg) in the range of -50 to -25°C. These mcl-PHAs are thermo elastomers with low crystallinity, low tensile strength and high elongation at break [26]. Scl-PHAs exhibit a broader range of properties depending on the monomer composition. For example, P(3HB) is of high crystallinity, brittle and stiff, and has the similar mechanical properties to those of polypropylene. Tm and Tg of PHB are 177°C and 4°C, respectively [27]; while P(4HB) has a Tm of 54°C and a Tg of -49°C [28]. The properties of PHAs vary considerably depending on their monomer composition.

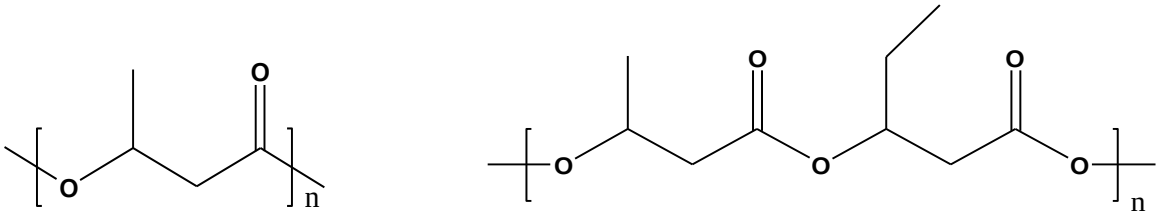

(a) (b)

Fig. 2-1. Chemical structures of some scl-PHAs: (a) PHB; (b) PHBV.

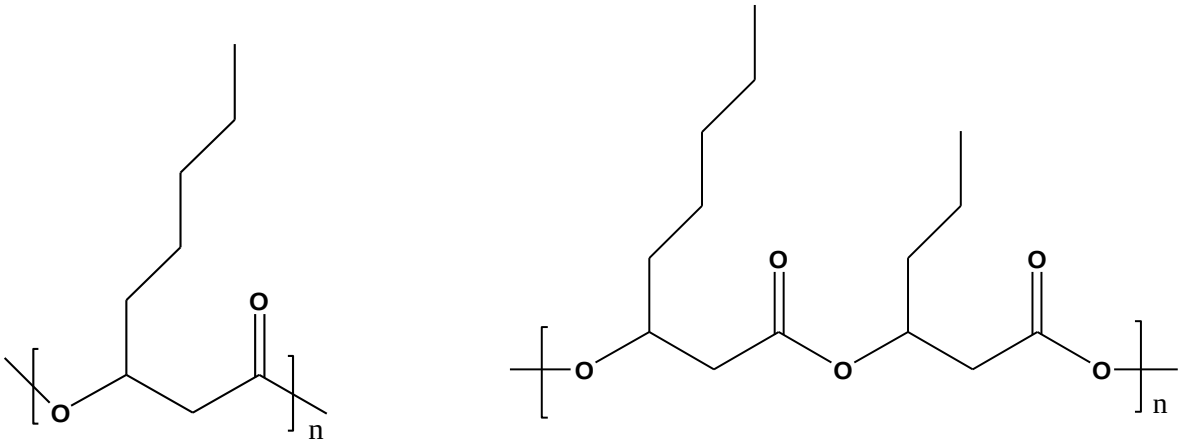

(a) (b)

Fig. 2-2. Chemical structures of mcl-PHAs: (a) PHO; (b) PHOHHx

2.2. The Biological Properties of Polyhydroxyalkanoate

2.2.1. Biocompatibility of PHAs

Biocompatibility has traditionally been concerned with implantable medical devices. Biomaterials used for implantable medical devices should be non-toxic, non-immunogenic, and non-irritant [29]. PHB, one of the most extensively investigated PHAs, has been found in many organisms, from bacteria to mammals [30]. PHB degradation will produce 3-hydroxybutyrate monomers, a natural metabolite associated with ketone body formation in animal cells [30].

Surface properties of various kinds of PHA films have been shown to be favourable for tissue cells proliferation and attachment, suggesting that PHAs are suitable candidates for tissue engineering scaffolds [31, 32]. P(3HB-co-3HHx)/P(3HB) scaffolds have shown strong growth and

proliferation of chondrocytes of rabbits [33, 34]. In a study conducted on mesenchymal stem cells (MSCs), P(3HB-co-3HHx) proved to promote and retain the chondrogenesis phenotype of MSCs [35]. Moreover, the effects of P(3HB) on different types of cells such as osteoblasts, fibroblasts, and chondrocytes, show desirable biocompatibility without causing any side effects [36]. Recently, mcl-PHA has been shown to be biocompatible with human mesenchymal stromal cells (hMSCs). An increase in proliferation of hMSCs was observed on mcl-PHA films, suggesting that the cell viability was not affected on mcl-PHA films [37].

2.2.2. Biodegradability of PHAs

One of the favorable properties of PHAs is its biodegradability: the cleavage of ester bonds in the backbone chains either hydrolytically or enzymatically. Some studies have investigated the biodegradation behavior of P(3HB), P(3HB-co-3HV), P(3HB-co-3HHx), and other PHAs. Lipases and some PHA depolymerases have been reported to degrade P(3HB-co-4HB) into 3-hydroxybutyrate and 4-hydroxybutyrate, which can be metabolized by the human body [38]. The biodegradation of P(3HB) has been tested in different cell lines targeted for use as implantable materials with various geometries, including films and plates [39-41], tubes [42, 43], thread-like filaments [44, 45] and microspheres [46]. In the human body, P(3HB) can be hydrolytically degraded to a normal blood constituent (D-(-)-3-hydroxy-butyric acid) of a concentration between 0.3 and 1.3 mM, so it has a potential application as a biomaterial [47]. P(3HB) implantation in the mandibular region of rats was investigated, and was found to be degraded within 6 months [48, 49]. However, because of high crystallinity P(3HB) degrades slowly. Other types of PHA, like PHBHV and PHBHHx, which have lower crystallinity and higher degradation rates when compared with P(3HB), are suggested as better candidates for tissue engineering scaffolds. PHBHV and PHBHHx were reported to be completely absorbed by rabbits [50]. Thus, the biodegradability property of various PHAs ensures that they can be used as biomaterials.

2.3. Theory of Electrospinning

2.3.1. Conventional Electrospinning.

Electrospinning is a method of creating continuous polymeric fibers with a diameter in the order of micro- or even nanometer by using electric fields [51]. The most basic electrospinning setup consists of three major components: a high voltage power supply, a syringe that holds the polymer solution with a needle as spinneret, and a collector separated at a defined distance (Fig. 2-3). When high voltage is applied between the spinneret and the collector, the electric field causes a surface charge repulsion of polymer solution, and the spherical drop of viscoelastic solution on the spinneret tip deforms into conical shape called a Taylor cone. When the electrostatic forces overcome the solution surface tension, a charged solution jet is ejected from the Taylor cone and is deposited on the surface of the collector. Simultaneously, with a rapid whipping of the jet, the solvents quickly evaporate and dried fibers are collected [51]. Electrospun nanofiber morphology can be tuned by varying: (1) the solution properties (i.e. the polymer concentration, viscosity, polymer molecular weight, solution conductivity); and (2) the electrospinning processing parameters (i.e. the applied voltage, solution feeding rate, and tip-to-collector distance).

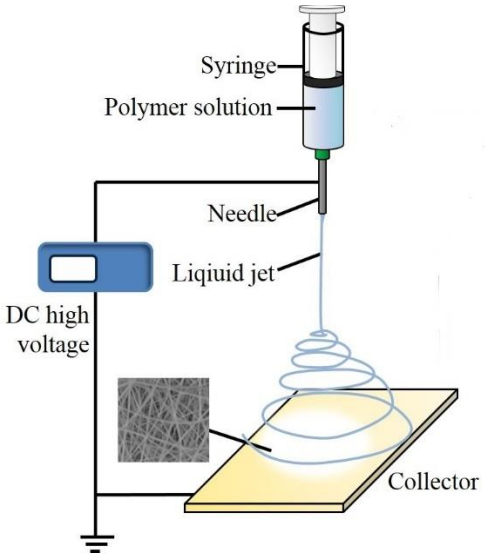

Fig. 2-3. Typical conventional electrospinning setup.

2.3.2. Coaxial Electrospinning.

With the relatively new technique of coaxial electrospinning, core-shell nanofibers can be fabricated using two different polymeric components. The general setup (Fig. 2-4), adopted by many researchers, is quite similar to that used for conventional electrospinning. However, coaxial electrospinning uses a coaxial nozzle: a central tube surrounded by a concentric circular tube. Different polymer solutions are fed into the coaxial nozzle separately, and ejected simultaneously. As in the conventional electrospinning, a Taylor cone is formed when a high voltage is applied between the spinneret and the collector, and a solution jet consisting of inner and outer solutions is ejected towards to the collector. Finally, the solvent evaporates, leading to the formation of core-shell nanofibers [52].

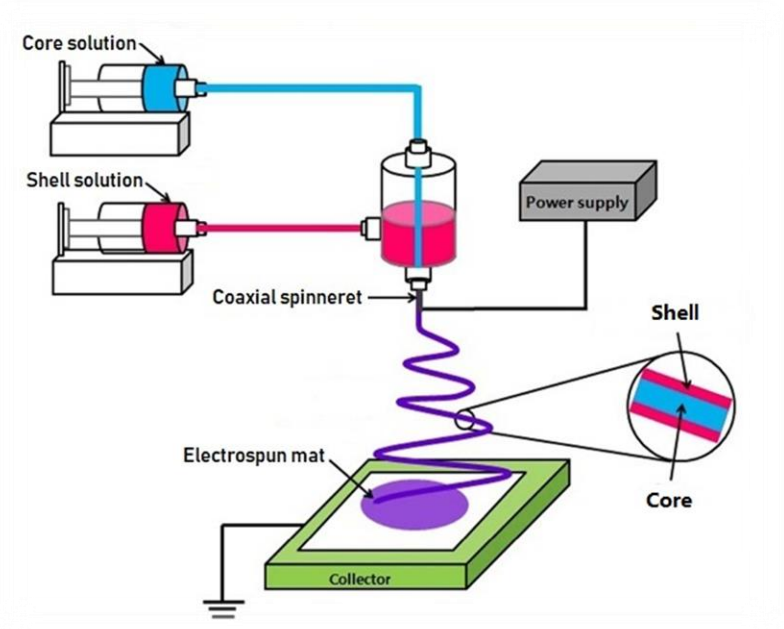

Fig. 2-4. Typical coaxial electrospinning setup.

2.4. PHA Electrospinning and Its Application in Biomedical field

To date, most electrospun PHA membranes reported have been made with scl-PHAs, including poly(3-hydroxybutyrate) (PHB) [53-55], poly(3-hydroxybutyrate-co-3-hydroxyvalerate) (PHBV) [56-58], poly (3-hydroxybutyrate-co-4-hydroxybutyrate) (P3HB-co-4HB) [55, 59], and poly (3-hydroxybutyrate-co-3-hydroxyhexanoate) (PHBHHx) [57, 60]. Table 2-1 reviews the electrospinning conditions for fabricating the electrospun PHA fibrous mats. Scl-PHAs are highly crystalline, making them rigid and brittle in nature, hence, they are not suitable for applications in contact with soft issues such as vascular applications, skin regeneration, or drug delivery systems [26]. In contrast, Mcl-PHAs are more elastomeric and flexible and thus may be used for soft tissue engineering. Moreover, because mcl-PHAs are more structurally diverse than scl-PHAs, they could provide more flexibility in tailoring the mechanical properties of mcl-PHAs to meet the requirements of different tissue engineering applications. In addition, mcl-PHAs have more amorphous regions where the hydrolysis of ester bonds usually occurs, which increases the *in vitro* and *in vivo* degradation rate [61]. However, pure mcl-PHAs also have their limitations with respect to electrospinning, due to their low glass transition temperatures and viscoelastic properties at room temperature. Mcl-PHAs electrospun fibers cannot retain their shape since they are tacky and sticky at room temperature.

Table 2-1. Electrospinning conditions for fabricating the electrospun PHA-fiber mats.

References	PHAs for electrospinning	Molecular weight (kDa)	Fiber diameters (nm)	Solvent	Polymer concentration (wt/vol)	Electrospinning conditions		
						Flow feeding rate (mL/h)	Collecting distance (cm)	Applied voltage (kV)
[62]	PHB PHBHV	144 84	420-4500	TFE	10% 15% 10%	1	25	25

	PHBHHx	200		80/20 vol% $CHCl_3$/DMF	14% 25%			
	PHOU	130			10%			
[57]	PHBHV PHBHHx PHOU	84 206 130	950±50 980±90	TFE	12.5% 10%	1.5	25	25
[58]	PHBHV	380 360 1900	319.6±836 4648±2312 3514±1585	TFE	6%	----------	10	40
[59]	P(3HB-co-4HB)	--------	150-200	50/50 vol% $CHCl_3$/DMF	20 %	----------	16	5~20
[63]	PHBHV	680	1000-4000	$CHCl_3$	2~23 wt.%	5	6–15	15–30
[53]	PHB PHBHV	300 680	2300 3700	$CHCl_3$	14%	---------- ----------	20	12
[54]	PHB PHBV	300 680	2300 3700	$CHCl_3$	14%	---------- ----------	20	12
[55]	PHB P(3HB-co-4HB)	1340 650	210±80 710±240	80/20 vol% $CHCl_3$/DMF	2-10%	2.4	20	10~30
[64]	PHBHV	----------	1270±210	80/20 vol% $CHCl_3$/DMF	10%	3	25	25
[65]	PHBV	----------	634-5947	$CHCl_3$	15%	1	15	15
[66]	PHBHV	310	2030-9710	$CHCl_3$	5-25%	1-9	12.5-30	2-25
[67]	PHBHV	----------	284-1166	$CHCl_3$	5-20%	----------	20-30	20-50
[68]	PHB PHBV	300 680	1600-6600	$CHCl_3$	10-16%	----------	15-25	8-14
[69]	PHBHHx	967 1210	430-1000	$CHCl_3$	2-5%	0.5	25	9-18

2.4.1. Electrospun PHAs as Tissue Engineering Scaffolds

Given the biodegradability and biocompatibility of PHA, an obvious biomedical application of electrospun PHAs matrix is for tissue engineering scaffolds. The applicability of electrospun fibrous mats of PHB, PHB-co-HV and their blends (PHB/PHB-co-HV 50:50) as tissue engineering scaffold material was assessed by indirect cytotoxicity evaluation according to ISO10993-5 standard test using L929 mouse fibroblasts [68]. None of the fibrous mats posed a threat to the cells and could be used as a scaffold for mammalian tissue culture. Direct cytotoxicity evaluation of these electrospun fibrous mats (PHB-co-HV, PHB, and their blends) was conducted with human osteoblasts (SaOS-2) by the same research group, and indicated biocompatibility of these materials to this type of cells [54]. The cells appeared to adhere well on all types of fibrous scaffolds after 16 hours of cell seeding. During the early stage of the proliferation period (from 24 to 72 hours in culture), the viability of the cells increased and appeared to be unchanged with further increases in the time in culture. The results implied a high potential of these electrospun fibrous mats for use as bone scaffolds [54].

Except for PHB-co-HV and PHB, P(3HB-co-4HB) and P(3HB-co-3HHx) were also electrospun to fabricate scaffolds with enhanced biocompatibility and bioabsorption [70]. After 12 weeks of implantation in rats, no fibrous encapsulation was observed around the degraded copolymer and there was a substantial drop in the number of inflammatory cells. Surface functionalization of PHA electrospun fibers was also reported to improve cell compatibility [57, 64]. Poly(3-hydroxyoctanoate-co-3-hydroxyundecenoate) (PHOU) with side epoxy groups (PHOUep) was chemically modified via the attachment of a peptide sequence, Arg-Gly-Asp, to obtain biomimetic scaffolds [57]. When compared with non-functionalized PHAs mats, these functionalized mats provided better adhesion with human mesenchymal stromal cells. A similar method incorporating a glycosaminoglycan-like marine exopolysaccharide HE800 to PHB-co-HV electrospun scaffolds for enhancement of cell adhesion was reported by [64]. Adhesion and growth

of human mesenchymal stem cells on the HE800 graft PHB-co-HV scaffolds showed a notable improvement over those on solely PHB-co-HV scaffolds. Based on these studies, PHAs electrospun mats were considered to be good candidates for tissue engineering scaffolds.

2.4.2. PHAs as Drug Delivery Systems

Given the numerous experimental evidences (in Section 2.2) that PHAs are tolerated well by the human body, electrospun PHAs have been studied for use as drug delivery systems. Paclitaxel, a lipophilic/hydrophobic drug for use as an anti-tumor agent for many cancers, was added into P(3HB-co-4HB) solution to produce bead-free electrospun nanofibers [55]. In preliminary drug release studies, the release pattern was consistent and controlled. P(3HB-co-4HB) drug loaded nanofibers have shown potential applications in the development of drug eluting stents by direct coating of a metal stent with a homogeneous layer of electrospun drug loaded polymer [55]. Another polymer, PHB, was investigated for drug release systems. Electrospun fibrous PHB with caffeic acid (CA) was found to kill *Staphylococcus aureus* and *Escherichia coli* and was effective in suppressing the adhesion of *S. aureus* [71]. PHAs have also been blended with other polymers for drug release systems. A blended electrospun fibrous mat of PHA copolymer and poly (butylene adipate-co-terephthalate) (PBAT) containing capsaicum extract was investigated for drug control release. The nanfibrous mats showed a potential for drug release patches [72]. Poly(hydroxybutyrate)/poly (ethylene oxide) (PHB/PEO) with chlorhexidine (CHX) exhibited significant bactericidal performance, where a reduction of 100% and 99.69% against *E. coli* and *S. aureus* respectively, was achieved, [73]. Therefore, PHAs electrospun mats were considered to be good candidates for drug release systems.

2.4.3. Electrospun PHAs as Wound Dressings

A wound dressing should be a 3D structure to support skin cells proliferation and differentiation. It also should keep its mechanical integrity and stability when placed onto a wound

site. PHB-co-HV, PHB-co-HV/collagen, and PHB-co-HV/gelatin electrospun nanofibrous mats were examined as dressings [74]. PHB-co-HV and PHB-co-HV/collagen mats cocultured with epithelial outer root sheath/dermal sheath cells for 3-5 days showed PHB-co-HV promoted wound closure, and could be used as a cell-seeded biological dressing [74]. Silk fibroin (SF) was also mixed with PHB-co-HV to improve the surface hydrophilicity and water-uptake capability of PHB-co-HV nanofibrous scaffolds [75]. The results of cell adhesion experiments showed that fibroblasts adhered more to the PHB-co-HV/SF electrospun scaffolds than to pure PHB-co-HV scaffolds. The proliferation of fibroblasts was higher on the PHB-co-HV/SF nanofibrous scaffolds than on pure PHB-co-HV nanofibrous scaffold, making PHB-co-HV/SF scaffold a possible candidate for skin tissue engineering and wound dressing [75].

Keratin, an important protein used for wound healing and tissue recovery, was blended with the same kind of PHA (PHB-co-HV) and electrospun to produce nanofibrous mats [76]. The composite mats accelerated wound recovery remarkably when compared to pure PHB-co-HV mats, which indicated that PHB-co-HV-keratin may be a good candidate for wound dressings [76].

Another PHA polymer, P(3HB-co-4HB), also has the potential for use as wound dressing. Nonwoven membranes of P(3HB-co-4HB) carrying the culture of allogenic fibroblasts was assessed against model skin defects in Wistar rats [77]. The wounds under the P(3HB-co-4HB) carrying cells healed 3.5 times faster than the wounds healing under eschar (control). An *in vivo* study showed that P(3HB-co-4HB)/collagen peptides had a significant effect on wound contractions, with a wound closure of 79% [77]. As stated above, PHAs nanofibrous mats prepared by electrospinning could be used as wound dressings for skin wound repair.

2.5. Polyhydroxyalkanoate Degradation by Lipases

Lipases are defined as hydrolases (EC 3.1.1.3) involved in the hydrolysis of acylglycerol into glycerol and free fatty acids in a lipid-water interface [78]. Under natural conditions, lipases

catalyze the hydrolysis of ester bonds (Fig 2-5). Many bacteria have been reported to produce lipase for the digestion of lipid materials, like *Pseudomonas fluorescents* [79], *Pseudomonas aeruginosa* [80], *Staphylococcus aureus* [81], *Streptococcus lactis* [82], *Achromobacter lipolyticum* [83], and *Myxococcus xanthus* [84].

.

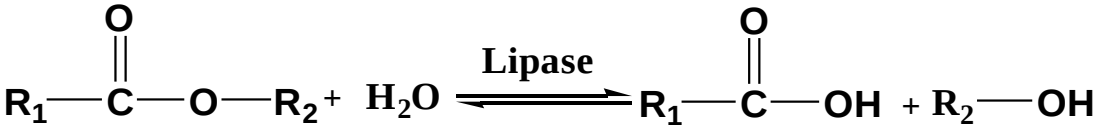

Fig. 2-5. Hydrolysis of ester bond by lipase.

The ester bonds between PHA monomers are known to be naturally hydrolyzed by some specific lipases, which are also named as PHA depolymerases. PHA depolymerase first binds on the materials surface, and then the hydrolysis occurs at amorphous region and subsequently at crystal region [85]. It is reported that eukaryotic lipases were more efficient in hydrolyzing PHA compared to prokaryotic lipases [86]. Poly(3-hydroxybutyrate-co-4-hydroxybutyrate) [P(3HB-co-4HB)] can be degraded by commercially available lipases [87].

Lipases from some fungi (such as *Candida antarctica, Candida rugosa*, and *Mucor javanicus*) and bacteria (such as *Pseudomonas cepacia* and *Pseudomonas fluorescens*) showed obvious depolymerizing activity. Surface morphology changes on P(3HB-co-4HB) film was observed using SEM after being degraded by *Pseudomonas fluorescens.* As lipase concentrations increased from 0.5 to 2.5 mg/mL, more holes were produced on the film (Fig 2-6) [87]. *Bacillus subtilis* DI2, a lipolytic strain, has been used for lipase-catalysed degradation of PHA [88].

The lipase-encoding gene from *Bacillus subtilis DI2* was PCR-amplified, cloned into a T-vector system and then sequenced. The lipase-encoding gene was expressed in *Escherichia coli*

cells and the recombinant lipase was purified for PHA degradation studies. After 72 h of incubation at 40 °C, it showed 21.3% and 28.3% molecular weight decrease and weight loss, respectively [88]. The degradation process of poly (3-hydroxybutyrate-co-3-hydroxyvalerate) (PHBV), the most common form of scl-PHA, was investigated in the presence of lipase (depolymerase) from *Pseudomonas lemoignei* [89]. Weight loss of PHBV copolymer films was monitored for the observation of PHA degradation. 2.6% per day was observed as the highest degradation rate [89].

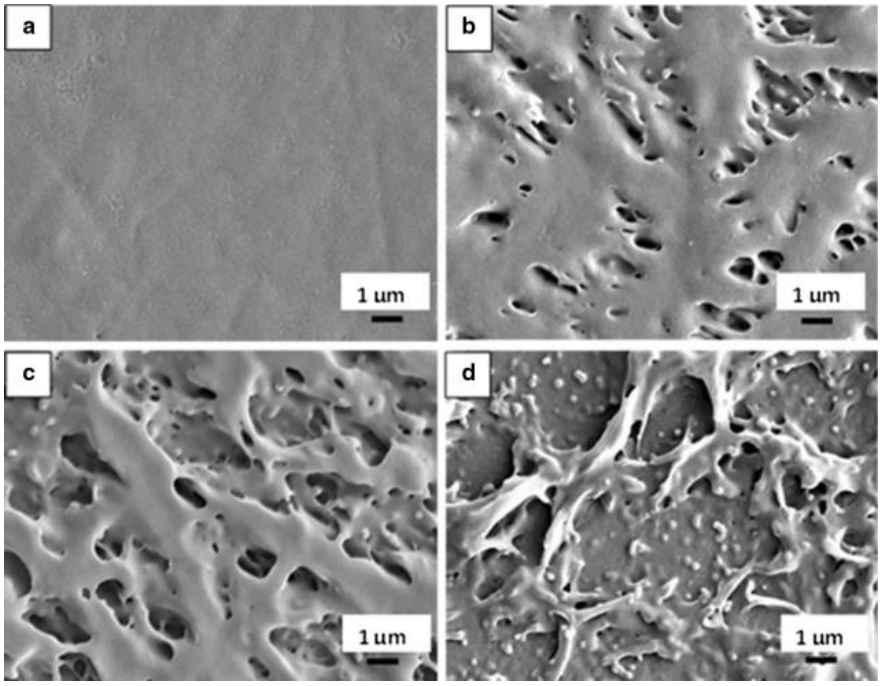

Fig. 2-6. SEM images of P(3HB-co-4HB) film after incubation with 10 μL of: (a) PBS; (b) lipase from *P. fluorescens* at 0.5 mg/mL in PBS; (c) at 1.0 mg/mL in PBS; and (d) at 2.5 mg/mL in PBS for 30 min at 37 °C.

3. Enabling Electrospinning of Medium-Chain Length Polyhydroxyalkanoates (PHAs) by Blending with Short-Chain Length PHAs

3.1. Introduction

Since pure mcl-PHAs have their limitations with respect to electrospinning, we investigated the use of blends of scl-PHA with mcl-PHA for electrospinning. To our best knowledge, only a few researchers have reported on blending scl-PHA with mcl-PHA for electrospinning [57, 90]. Azari et al. [90] blended brittle PHB with a palm oil-based mcl-PHA to improve its mechanical properties, but either micro-size fibers were obtained at lower percentage of mcl-PHA, or beaded nanofibers were fabricated at higher percentage (30-40 wt%). Hence the PHB/mcl-PHA electrospun membranes with this morphology were not suitable for soft tissue engineering in nanometer scale. Ramier et al. [57] blended poly (3-hydroxyoctaanoate-co-3-hydroxyundecenoate) modified with side epoxy groups with PHBHHx to facilitate electrospinning process. But no detail was provided on how mcl-PHA incorporation influenced the physical and mechanical properties of the PHBHHx nanofibrous mat.

In this study, we blended PHBV25 (consisting of 75 mol% 3-HB and 25 mol% 3-HV) with PHOHHx (with HO content of 92.6 mol% and HHx content of 6.1 mol%) for electrospinning, and comprehensively investigated the effects of various solution properties and processing parameters on morphology of the electrospun nanofibers. The viscosity based average molecular weights of PHBV12, PHBV25 and PHOHHx were characterized by intrinsic viscosity [η] (dl g-1). Rheological principles were utilized in the investigation of electrospinnability of PHBV25 and PHOHHx. The morphology of electrospun membranes were investigated by means of scanning electron microscopy (SEM). In order to explore the potentials of PHBV25/PHOHHx nanofibrous membranes in soft tissue engineering, wide-angle X-ray diffraction (WAXD), differential scanning calorimetry (DSC), Fourier transform infrared spectroscopy (FTIR) and tensile test were utilized

to characterize PHBV25/PHOHHx nanofibrous membranes crystalline structure, crystallinity, chemical structure and mechanical properties, respectively. PHBV25 and commercially available PHBV12 were chosen as comparison with blends of PHBV25/PHOHHx.

3.2. Materials and Methods

3.2.1. Materials

PHBV25 and PHOHHx (defined above) were produced by Dr. Levin's group in the Department of Biosystems Engineering at the University of Manitoba, Canada. PHBV12 (with a 3-HB content og 9 mol% and a 3-HV content of 12 mol %) was purchased from Sigma-Aldrich, Canada. All the PHAs were purified before use. Briefly, the purification was performed by dissolving PHAs in chloroform followed by precipitation in methanol and filtration. Mixture of chloroform (CHCl3) and dimethyl formamide (DMF) was used as the solvent (80/20 vol%). Both were purchased from Sigma-Aldrich, Canada.

3.2.2. Molecular Weight Determination

The average molecular weight of PHBV25 and PHOHHx was characterized by intrinsic viscosity [η] (dl g-1). Viscosimetric measurements were performed in a chloroform solution at 30 °C by Ubbelohde's viscometer. The mean molecular weight is calculated according to the Mark-Houwink equation $[\eta] = KM^{\alpha}$, where [η] is the intrinsic viscosity and K and α are the constants for the given polymer-solvent system. For PHBV, $K = 1.18 \times 10^{-4}, \alpha = 0.78$ [91, 92]. For PHOHHx, $K=1.70\times10^{-4}$, α=0.701 [93].

3.2.3. Steady Shear Rheology

Molecular entanglement of polymers in the spinning solution is an essential prerequisite for successful electrospinning. Rheology study can be a powerful tool to probe molecular conformation and interaction in polymer dispersions, and studies were performed using a TA

Instruments AR 2000 rheometer with the following experimental parameters: shear rate from 50 to 1300 s^{-1}, PHOHHx and PHBV25 solutions ranging from 0.5 to 50% (w/v) and 0.5 to 15% (w/v), respectively in a $CHCl_3$/DMF (80/20, v/v) solvent at 25 ± 0.2°C. Specific viscosities were plotted as a function of concentration, and were used to identify semi-dilute un-entangled and semi-dilute entangled regimes. The semi-dilute un-entangled regime had a small slope, while the semi-dilute entangled regime had a greater slope. The intersection of the two fitted lines was the entanglement concentration, ce.

3.2.4. Preparation of Spinning Solutions

PHBV12, PHBV25, PHOHHx and PHBV25/PHOHHx spinning solutions were prepared in $CHCl_3$ /DMF (80/20 vol%). PHBV12 and PHBV25 were dissolved at concentrations of 17% and 15% (w/v) respectively. The weight compositional ratios between PHBV25 and PHOHHx in the blend solutions were 50/50, 55/45, 60/40, 65/35, 70/30, and 75/25, respectively. These solutions were vigorously stirred with a magnetic stir bar for at least 5 hours at 50 °C to ensure homogeneity.

3.2.5. Electrospinning

The electrospinning apparatus NE 300 (Inovenso Ltd. Co, Turkey) consisted of a high voltage power supply, syringe pump, and a grounded plate collector arranged in a horizontal configuration. A 6 mL syringe containing the polymer solution was loaded into the syringe pump, and a nozzle with an inner diameter of 0.8 mm was attached to the syringe through a high-density polyethylene tube. The electric field was applied by means of a high voltage supply capable of delivering up to 40 kV with respect to ground. The electrospun mats were collected onto a grounded plate collector (diameter of 10 cm). In this study, the effects of polymer concentration, applied voltage between nozzle tip and collector, and polymer solution feeding rate on PHBV25/PHOHHx nanofibers morphology were investigated. The temperature was kept at room temperature, and the tip-to-collector distance was kept at 20 cm during the operation of the electrospinning process.

Electrospun mats were carefully detached from the collector and dried in vacuum oven at room temperature for 48 h to remove residue solvent.

3.2.6. Morphology of As-spun Nanofibrous Mats

The morphological appearance of the as-spun nanofibers was observed with a FEI environmental scanning electron microscope (Quanta 650 FEG) after sputter-coating with gold for 30 s. The morphology of electrospun nanofibers was observed from SEM pictures. The average diameter and the diameter distribution were measured by Image J software from SEM pictures in original magnification of 5K× and10K× with the average values being calculated from at least 100 measurements.

3.2.7. Crystallinity of PHAs Mats

Crystallinity was determined by both differential scanning calorimetry (DSC) and wide angle X-ray diffraction (WAXD). The melting enthalpy, ΔHm, was measured by DSC Q200 (TA Instruments, New Castle, DE, USA). Samples were sealed in aluminum pans and weights of approximate 6 mg were used. Under a nitrogen atmosphere, PHBV25/PHOHHx samples were scanned from -40 °C to 200 °C with a rate of 10 °C/min, while scan ranges for PHBV and PHOHHx were from -20 °C to 200 °C and -40 °C to 90 °C, respectively. The crystallinities of the PHA membranes were determined using Eq. (1), where ΔH_f is apparent melting enthalpy, ΔH_f^{ref} is the melting enthalpy for 100% crystalline PHB (146 J/g) and W_f is the weight fraction of PHBV [94, 95].

$$\text{Crystallinity} = \left[\frac{\Delta H_f}{\Delta H_f^{ref} \times W_f}\right] \times 100 \qquad (1)$$

WAXD patterns of various PHAs membranes were acquired using an X-ray diffractometer (RINT UltraX 18, Rigaku Japan). Ni-filtered Cu radiation (λ=0.1542 nm) was generated at 40 kV and 30 mA. The diffraction angle (2 theta) was scanned from 8° to 36° with a rate of 1°/min.

Crystallinity % of the polymer was calculated as a ratio of the total area of crystalline peaks to the total area of the radiograph (the crystalline and amorphous components) by using MDI Jade 6.

3.2.8. Fourier Transmission Infrared Spectroscopy (FTIR)

An ATR-FTIR spectrometer (Thermo Scientific™ Nicolet™ iS™10 FT-IR Spectrometer) is a reliable and cost-effective analytical tool for identification and assessment of quality of polymers. It is used to obtain an infrared spectrum of absorption of a polymer sample. The ATR-FTIR spectra of materials were evaluated in the range of 3100 to 500 cm^{-1} with a resolution of 4 cm^{-1} at 32 scans.

3.2.9. Mechanical Tests

Mechanical properties in terms of tensile strength, Young's modulus, and elongation at break were measured by using an Instron tester (3366 dual column tabletop testing system). The dimensions of samples with dimensions of 40 mm × 5 mm were cut out from electrospun mats. The apparent thickness of the membranes was determined by a digital vernier caliper. The apparent thickness was in the range of ~ 0.1 mm to 0.3 mm. Samples were fixed with two clamps in a vertical position and preloaded at 0.01 N. After the preloading, the force was set to zero and a constant crosshead speed of 10 mm/min was determined. Data were collected until the sample's rupture. Strain-stress curves were recorded. Computer software NEXYGEN PLUS provided the tensile strength (MPa), the percentage elongation at the break moment (%) and Young's modulus (MPa). Five independent replicated experiments were conducted for each condition tested, and the results were expressed as the means ± standard error.

3.3. Results and Discussion

3.3.1. Molecular Weight of PHBV12, PHBV25, and PHOHHx

Commercially available PHBV12 and PHAs recovered from bacteria cultures were purified to determine their molecular weight. Table 3-1 presents the intrinsic viscosity and molecular weight of PHBV12, PHBV25 and PHOHHx polymers. Molecular weight of PHBV25 was the highest, and

PHOHHx had the lowest molecular weight. Molecular weight of the three PHAs are higher than 84 kDa, the molecular weight threshold at which uniform bead-free nanofibers can be possibly fabricated via electrospinning of PHAs based on our literature review [57, 62].

Table 3-1. Intrinsic viscosity and viscosity average molecular weight of PHBV25 and PHOHHx.

	[η] (dl g-1)	Molecular Weight (kDa)
PHBV12	1.224	141
PHBV25	1.46-1.51	174-186
PHOHHx	0.538-0.541	98-99

3.3.2. Solution Rheology and Determination of Concentration Regimes for PHBV25 and PHOHHx

Entanglement concentration (ce) is the boundary between the semi-dilute un-entangled and semi-dilute entangled regimes. The polymer concentration has to be higher than the entanglement concentration for successful electrospinning. McKee [96] investigated the relationship between solution rheology and electrospun fiber formation of polyesters. Entanglement concentration (ce) was the minimum concentration required for electrospinning of beaded fibers, while 2-2.5 times ce was the minimum concentration required for electrospinning of uniform, bead-free fibers.

Our analyses revealed that, PHOHHx required a higher concentration (29%, w/v) than PHBV 25 (7.4%, w/v) to start entangling (Fig. 3-1). Two reasons may explain this: first, for polymers with similar molecular weights, the entanglement concentration is higher for branched polymers since branching hinders chain entanglements and overlaps. Second, the molecular weight of PHOHHx is almost half of that of PHBV 25.

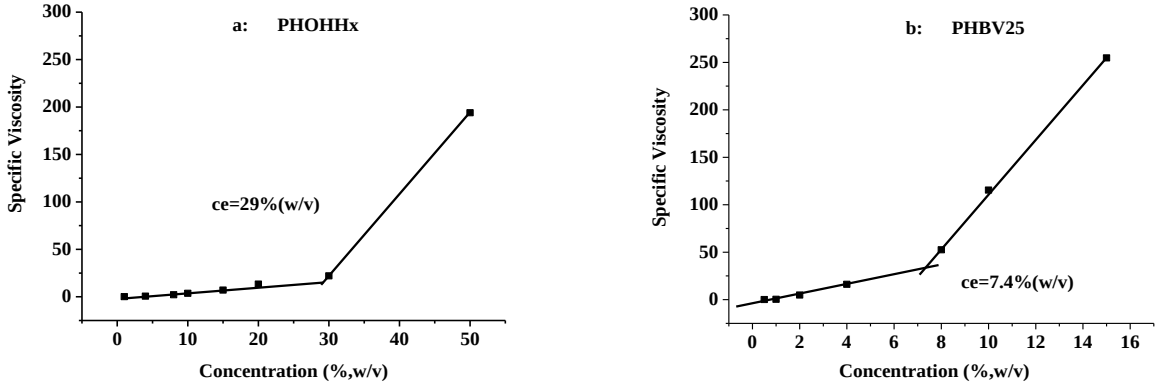

Fig. 3-1. Dependence of specific viscosity on concentration for: a) PHOHHx and b) PHBV25.

3.3.3. Electrospinnability of PHBV12, PHBV25, and PHOHHx

By varying the concentration of polymer solutions, electrospun nanofibers were obtained at 17% and 15% (w/v) for PHBV12 and PHBV25 solutions. At higher concentrations, the viscous solution may become solidified during the electrospinning process, which would hamper the continuity of electrospinning. The morphology of PHBV12 and PHBV25 nanofibrous mats are presented in Fig. 3-2. This result was consistent with the molecular weight of PHBV12 and PHBV25. PHBV12 and PHBV25 have similar chemical structure, but the molecular weight of PHBV25 was higher than that of PHBV12, so it required a higher concentration to obtain bead-free PHBV12 nanofibers.

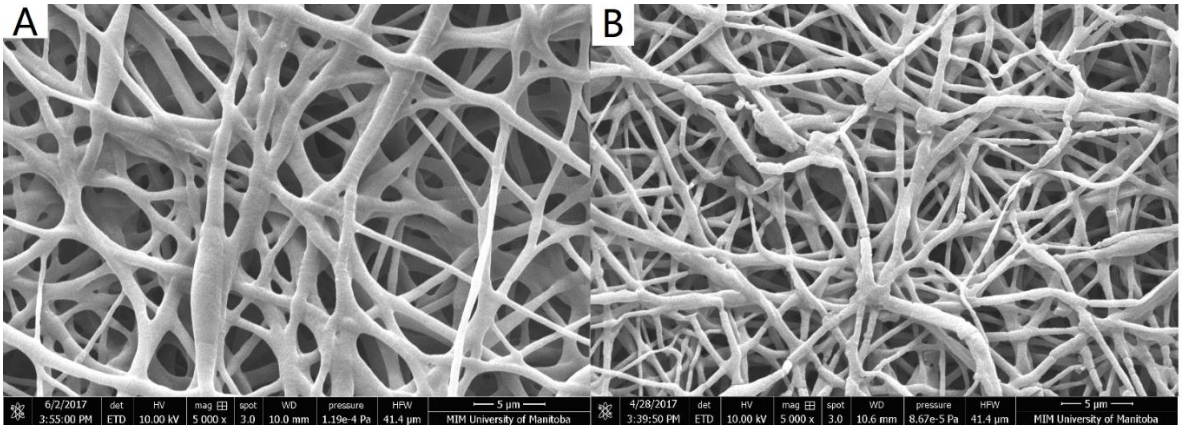

Fig. 3-2. Morphology of electrospun A) PHBV12 and B) PHBV25 at 17% and 15%(w/v).

Unlike PHBV12 and PHBV25, PHOHHx cannot be smoothly electrospun into nanofibrous mats, even if the polymer solution was prepared at 50% (w/v), which fell in the semi-dilute entangled regimes according to the specific viscosity versus concentration curve of PHOHHx (Figure 3-1 a). At the beginning of electrospinning (within 1 minute), fibrous features were observed on the plate collector, and as the electrospinning process continued, the fibrous features gradually faded away, followed by formation of a "wet" film consisting of a network of fibers fused together after 4 minutes (Fig. 3-3).

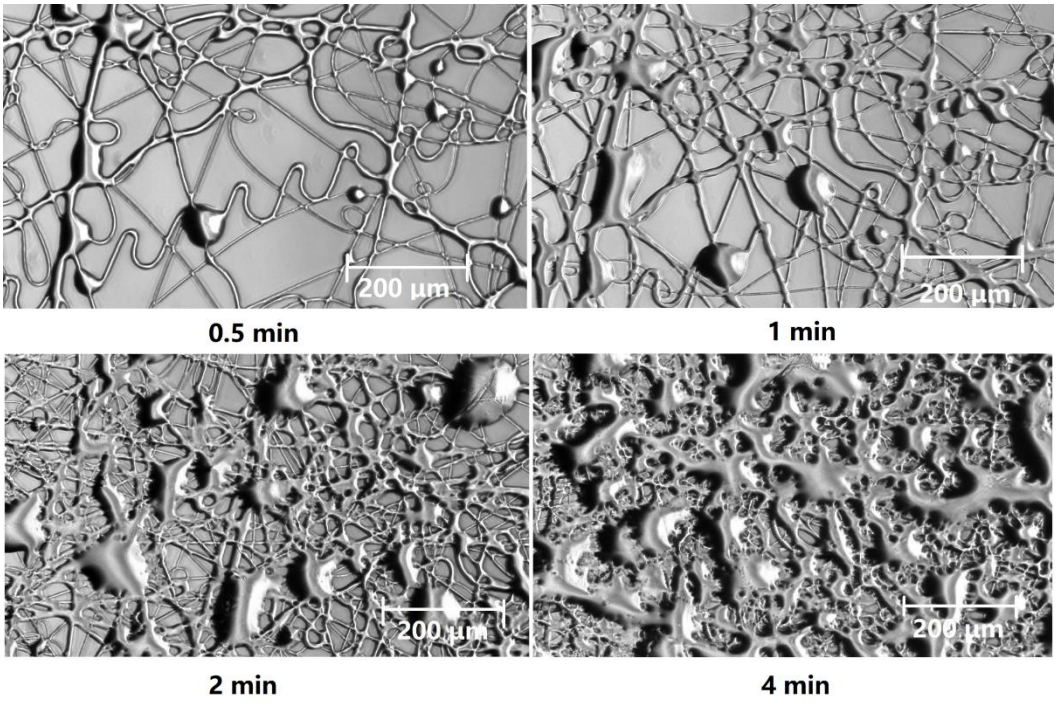

Fig. 3-3. Changes in PHOHHx fiber morphology as a function of time observed under optical microscope.

3.3.4. Electrospinning of PHBV25/PHOHHx

To facilitate the PHOHHx electrospinning process, it was blended with PHBV25 by dissolving it in $CHCl_3$/DMF (80/20 vol%) at different ratios (PHBV25/PHOHHx=50/50, 55/45, 60/40, 65/35, 70/30, and 75/25) at a fixed polymeric concentration of 15% (w/v). Nanofibers morphology gradually changed as shown in Fig. 3-4. As the ratios of PHBV25/PHOHHx increased from 50/50 to 75/25, the fibrous features gradually became more stable. When the ratio of PHBV/PHOHHx composite was 50/50 and 55/45, there was no sign of nanofibers. Fibers fused together to form a "wet membrane". At ratio of 60/40, fiber fusing was not as severe. At the ratios of 65/35 and 70/30, the nanofibers were much more uniform, fiber fusion was not observed, and smooth, bead-free electrospun nanofibrous mats were obtained. The electrospun mats had the greatest uniformity of nanofibers at a ratio of 75/25.

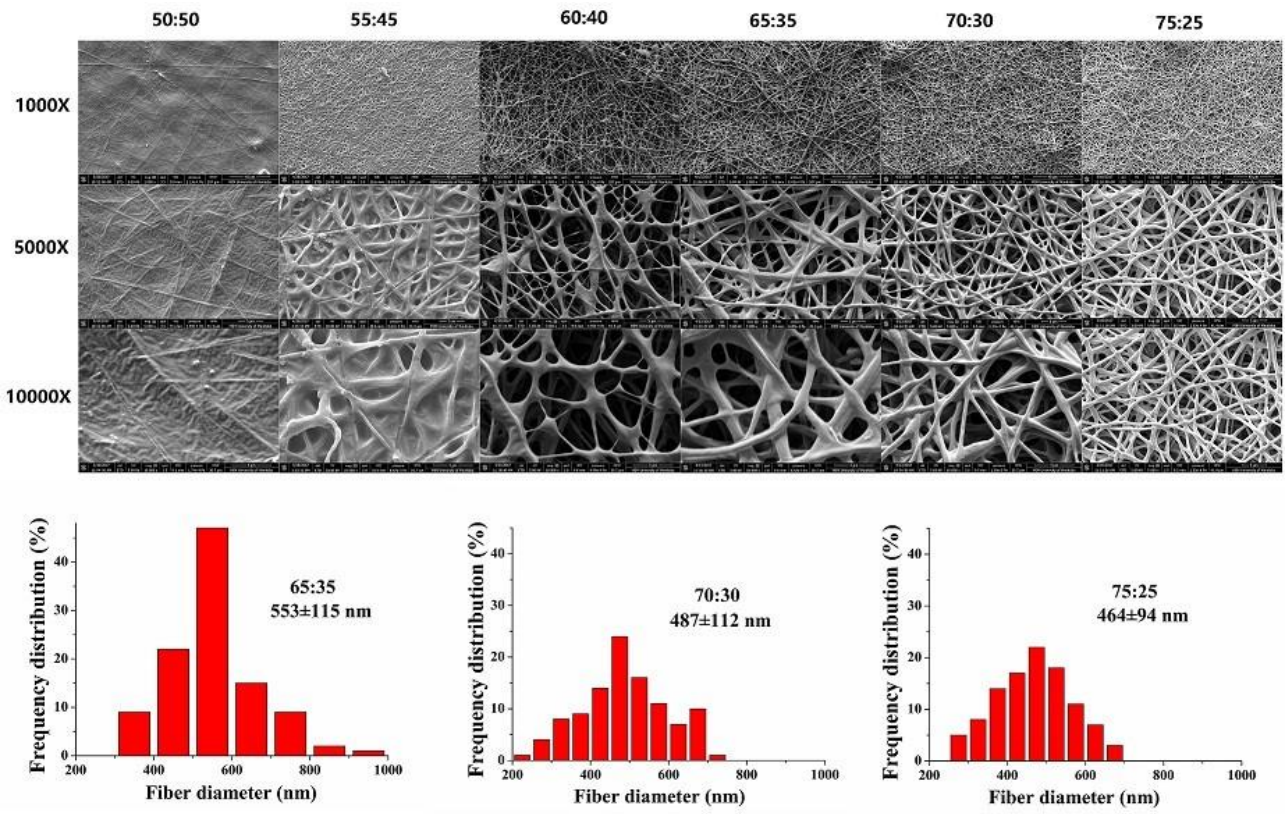

Fig. 3-4. Morphology and nanofiber diameter distribution of electrospun PHBV25/PHOHHx at ratios of 50/50, 55/45, 60/40, 65/35, 70/30, and 75/25.

3.3.5. Effects of Processing Parameters on Morphology of PHBV25/PHOHHx (75/25 wt%) Nanofibrous Mats

3.3.5.1. Effect of concentration on nanofibers morphology

Morphological changes were found when the total polymeric concentration of PHBV25/PHOHHx (75/25 wt%) was changed. The SEM images of the electrospun nanofibrous mats from PHBV25/ PHOHHx solution with different concentrations, at a voltage of 29 kV and a flow rate of 1 mL/h, are shown in Fig. 3-5. At lower concentrations (7.5% and 10%, w/v), bead-fibers could be attributed to lower viscosity of the PHBV25/PHOHHx solution. As the concentration increased from 10% (w/v) to 12.5% (w/v), the entanglement of polymer molecular

chains became more significant and prevented the break-up of the jet, allowing further elongation of the jet. Fewer beads were observed under these conditions. At 15% (w/v), smooth bead-free electrospun nanofibrous mats were obtained. At concentrations higher than 15% (w/v), the viscous solution became solidified during the electrospinning process, which hampered continuous electrospinning.

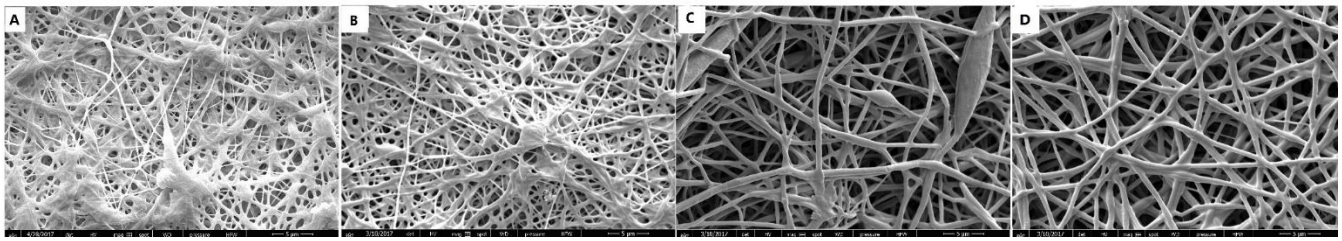

Fig. 3-5. Concentration effect on microstructures of electrospun PHBV25/PHOHHx nanofibers at voltage of 29 kV, with a feeding rate of 1 ml/h, and concentration of A) 7.5% (w/v); B) 10 % (w/v); C) 12.5 % (w/v); and D) 15 % (w/v).

3.3.5.2. Effect of applied voltage on nanofibers morphology

Increasing voltage resulted in greater stretching of the electrospinning jet and thus in turn to thinner fibers, with fewer and smaller beads. Five voltage levels were selected for production of the nanofibers: 15.5, 20, 24.5, 29, and 33.5 kV. Other parameters, such as concentration and feeding rate were kept constant at 15% (w/v) and 1 mL/h, respectively. Average diameter was calculated from at least 100 measurements ($n > 100$). Nanofiber morphology and average diameter distribution at various applied voltages were shown in Fig. 3-6.

At 15.5 kV, significant numbers of beads were observed because of insufficient electric field force to stretch the electrospinning jet. The average diameter of nanofibers was the highest, at 661 ± 233 nm. As the voltage increased to 20 kV, the nanofibers were subjected to greater stretching force, hence the beads size and average diameter of nanofibers decreased. From 24.5 to 29 kV, bead-nanofibers were seldom observed and the average nanofiber diameter decreased to 465 ± 94

nm. The diameter distribution also narrowed. When voltage was increased to 33.5 kV, the average diameter of nanofibers was 413 ± 128 nm.

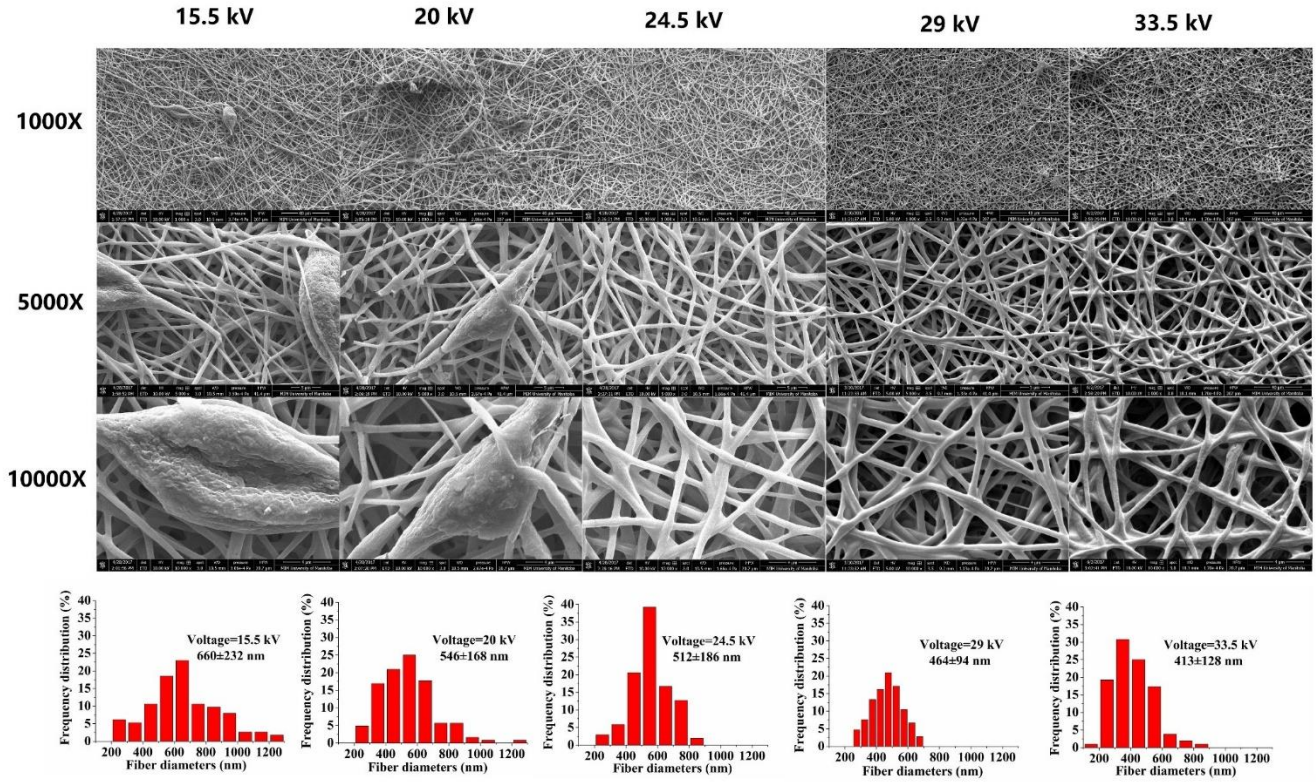

Fig. 3-6. Applied voltage effect on microstructures of electrospun PHBV25/PHOHHx (75/25 wt%) nanofibers at concentration of 15% (w/v), feeding rate of 1 ml/h, and voltage of 15.5, 20.0, 24.5, 29.0, and 33.5 kV.

3.3.5.3. Effect of solution feeding rate on nanofibers morphology

A certain minimum solution volume should be maintained at the end of the spinneret in order to form an equilibrium Taylor cone. Therefore, morphology of obtained nanofibers might vary with changes in the solution feeding rate at a given electric field. At 0.5 mL/h, the rate at which the polymer solution was electrospun was higher than the feeding rate. The electrospinning process was not continuous, and this may hinder the efficiency of electrospinning. At 1 mL/h, a balance

was achieved between the rate of solution consumption and the solution feeding rate. A single electrospinning jet was observed. As feeding rate was increased to 2 mL/h and 4 mL/h, dual-jets were occasionally observed.

It was found that the lower the solution feeding rate, the smaller the formed nanofibers. When feeding rate was 0.5 mL/h and 1 mL/h, the average diameters of nanofibers were almost the same, 479 ± 155 nm and 465 ± 94 nm, respectively (Fig. 3-7). When feeding rate increased to 2 mL/h and 4 mL/h, higher average diameters with wider diameter distribution were observed, 690 ± 229 nm and 761 ± 204 nm, respectively.

This behavior could be explained as follows. As the feeding rate increased under a constant voltage, the Taylor cone became bigger, and the size of Taylor cone determined the diameter of initial jets. Fibers with a larger diameter were expected. Also, as the Taylor cone became bigger, a dual-jet could occur and electrospinning jet became unstable, and jet instability favoured a wider diameter distribution.

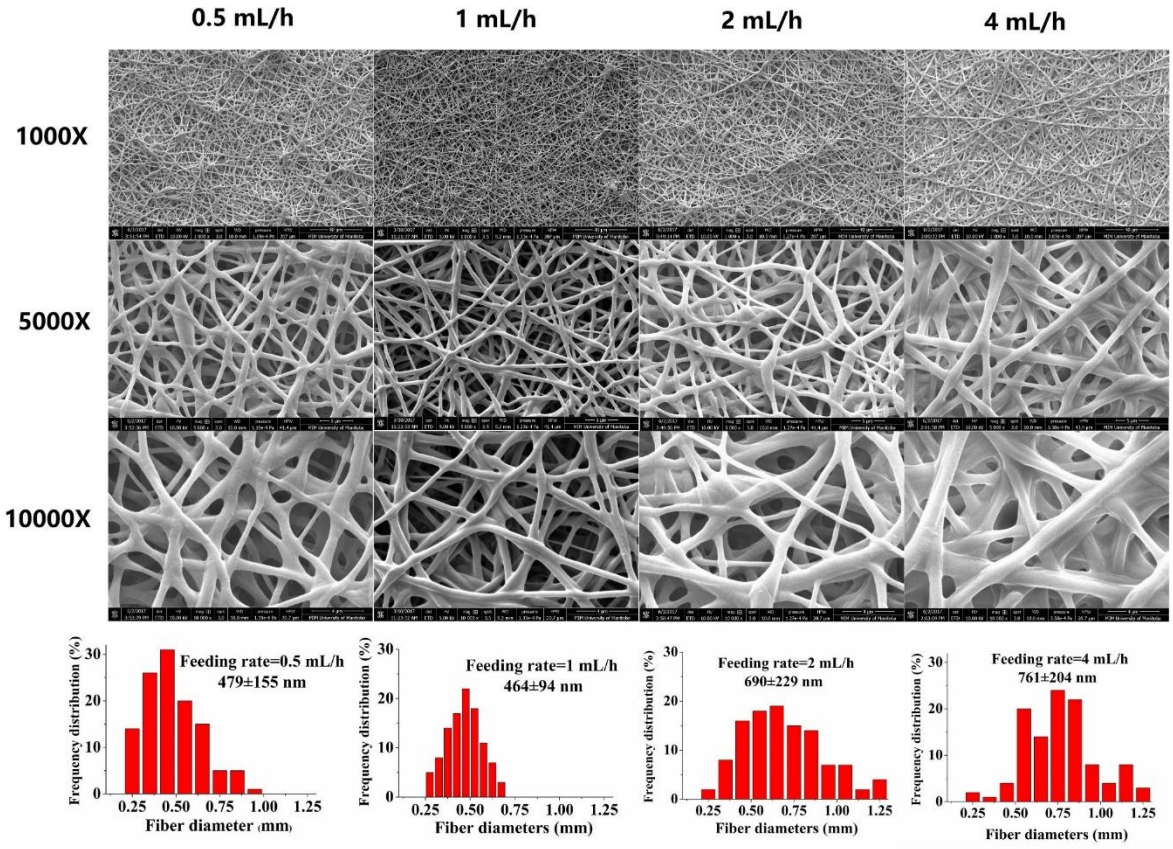

Fig. 3-7. Feeding rate effect on microstructures of electrospun PHBHV25/PHOHHx (75/25 wt%) nanofibers at concentration of 15% (w/v), voltage of 29 kV, and feeding rate of 0.5, 1, 2, and 4 mL/h.

3.3.6. Crystallinity of PHAs Mats

The crystalline properties of the electrospun fibers are important in practical applications. PHB is a homopolymer that is a hard and brittle material due to its high crystallinity. When small amounts of 3-hydroxyvalerate are randomly incorporated into PHB to form a copolymer, the 3-hydroxyvalerate monomers act as impurities and are excluded from the PHB crystalline lattice in PHBV [97]. Fig. 3-8 presents DSC data for various PHAs electrospun and cast membranes.

Melting enthalpy and crystallinity data are shown in Table 3-2. PHBV12 had a higher crystallinity than PHBV25, both in cast and electrospun membranes, and it was attributed to the 3HV units inhibiting the polymer crystallization through hydrogen bonding [98, 99]. When PHBV25 was mixed with PHOHHx at a ratio of 75/25 (wt%), the crystallinity of the blends decreased. PHBV12, PHBV25 and PHBV25/PHOHHx cast membranes presented two melting peaks, a melting shoulder followed by a sharper melting peak. The appearance of two melting peaks has been reported for several PHBV polymers [58, 99, 100]. During the course of melting, some defective or smaller crystals melted and then recrystallized, forming more perfect crystals which subsequently melt at higher temperature [99, 100]. Nanofibrous membranes made from electrospun PHBV12, PHBV25, and PHBV25/PHOHHx (75/25 wt%), had relatively lower crystallinity when compared with cast membranes. The slight decrease in crystallinity of electrospun membranes was due to the rapid evaporation of solvent, which hindered the formation of nuclei and the growth of a crystal grain. This also hindered the two-step melting behaviour.

PHBV12 and PHBV25 cast or electrospun membranes showed similar XRD spectra and presented diffraction peaks at around 2θ=13.6°, 17.1°, 26.1°, 27°, and 30.5°, ascribable to the helix lamellar -form conformation of the PHB and to the (020), (110), (121), (040) and (002) crystallographic planes (Fig. 3-9). PHBV12 has a higher crystallinity than PHBV25, both in cast and electrospun membranes, because of less 3-hydroxybuterate incorporation. PHOHHx cast membranes showed a highly amorphous broad-band with percentage of crystallinity of only 10.3%. When PHBV25 was mixed with PHOHHx at a ratio of 75/25 (wt%), the crystalline structure did not change appreciably.

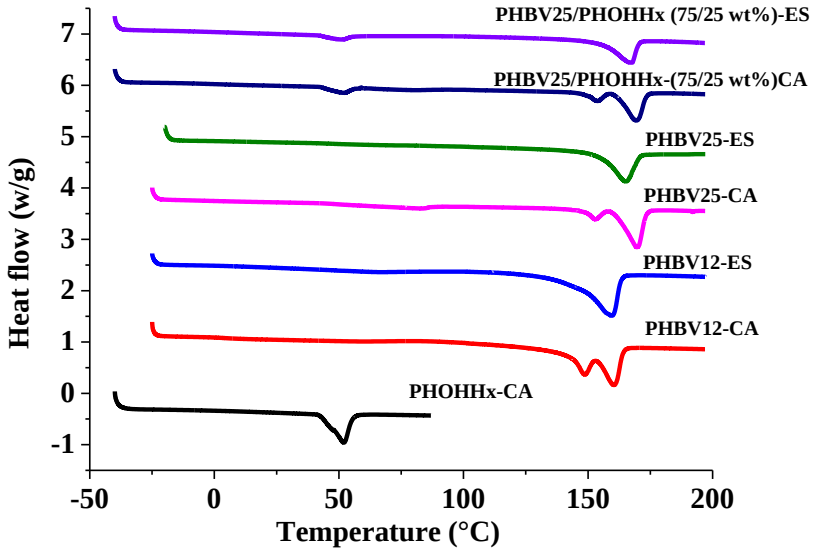

Fig. 3-8. Differential scanning calorimetry results of various PHAs membranes. CA refers to cast membrane; ES refers to electrospun membrane.

For PHBV12, PHBV25 and PHBV25/PHOHHx (75/25 wt%), their electrospun membranes have relatively lower crystallinity when compared with cast membranes. The crystallinity for PHBV12, PHBV25, and PHBV25/PHOHHx (75/25 wt%) cast membranes were 29%, 26.4%, and 20%, respectively, while those of their electrospun membranes were 26.2%, 20.5%, and 16.1%, respectively (Table 3-2). Crystallinity trends of different PHAs membranes obtained from XRD spectra are consistent with that obtained from DSC patterns. Since the mechanisms behind polymer crystallinity prediction using DSC and XRD are quite different, the differences resulted from these two methods were always observed for semicrystallinine polymers [101]. DSC crystallinities were slightly higher than XRD ones, which may be due to small crystals generating changes in the thermodynamic heat of fusion in DSC, while XRD may require a larger crystal size and longer range order [102].

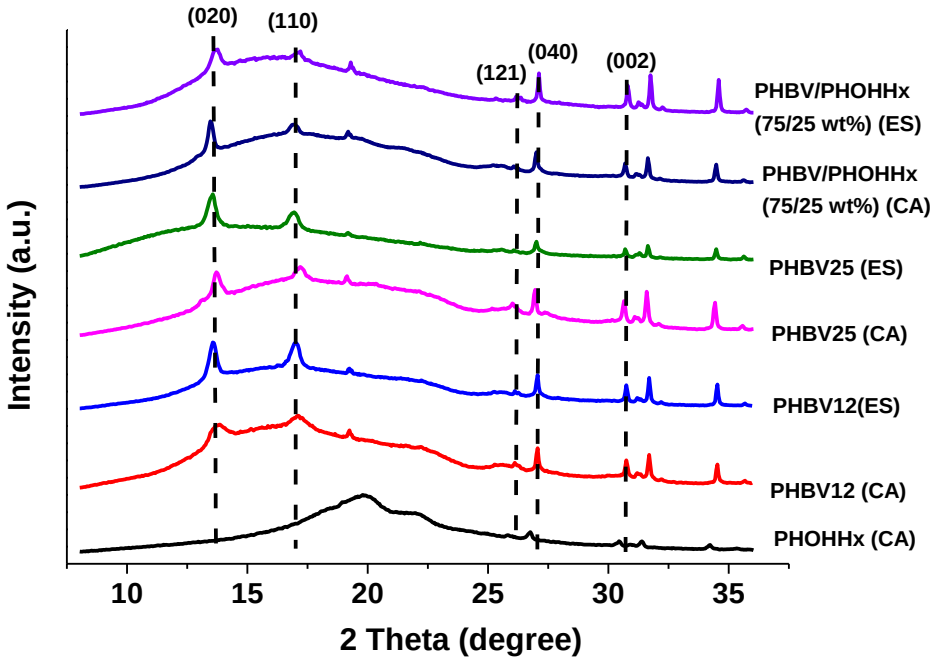

Fig. 3-9 X-ray diffractograms of the different PHAs membranes. CA refers to cast membrane; ES refers to electrospun membrane.

Table 3-2 Melting enthalpy and crystallinity % of various PHA membranes.

	Melting enthalpy (J/g)	Crystallinity % obtained from DSC	Crystallinity % obtained from XRD
PHOHHx cast membrane	23.43	16.0	10.3
PHBV12 cast membrane	66.48	45.5	29.0
PHBV12 electrospun membrane	60.29	41.3	26.2
PHBV25 cast membrane	41.41	28.4	26.4
PHBV25 electrospun membrane	37.31	25.6	20.5
PHBV25/PHOHHx (75/25, wt%) cast membrane	28.84	26.3	20.0
PHBV25/PHOHHx (75/25, wt%) electrospun membrane	25.07	22.9	16.1

3.3.7. Chemical Characterization of PHAs Mats

FTIR is sensitive to conformational and local molecular environment of polymers, and it has been extensively used as a convenient and powerful tool for investigating the chemical structure of polymers. The ATR-FTIR spectra from 500 cm^{-1} to 3100 cm^{-1} of PHBV12, PHOHHx, PHBV25 and PHBV25/PHOHHx (75/25, wt%) membranes are shown in Fig. 3-10. The C=O stretching vibration of PHBV12, PHBV25, PHOHHx and PHBV25/PHOHHx (75/25, wt%) present strong peaks at 1717 cm^{-1}, 1720 cm^{-1}, 1726 cm^{-1}, and 1720 cm^{-1}, respectively. Peaks between 3000 cm^{-1} and 2800 cm^{-1} are assigned to aliphatic C-CH_3 stretchings of alkyl chain of PHA. An aliphatic C-CH_3 bending presents at around 1379 cm^{-1} for all four types of membranes. The C–O stretching vibration bands of PHBV12 and PHBV25 are placed at 1229 cm^{-1}, 1276 cm^{-1} and 1228 cm^{-1}, 1277 cm^{-1}, while for PHOHHx the C–O stretching bands present at 1317 cm^{-1}, 1161 cm^{-1}, and 1097 cm^{-1}. And a skeletal vibration of –$(CH_2)_4$–shows at 725 cm^{-1} for PHOHHx [103-105]. By blending PHOHHx and PHBV25, no new peaks appeared, which means there was no new chemical groups formed after blending.

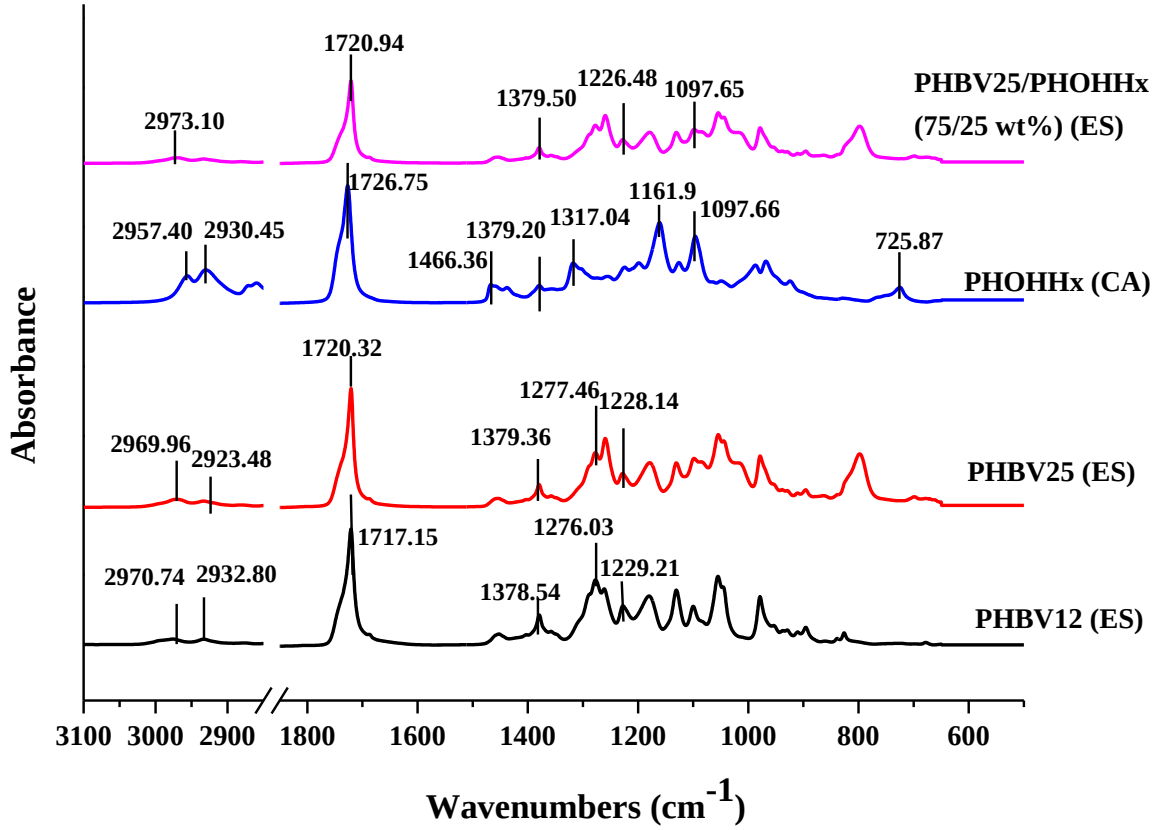

Fig. 3-10. ATR-FTIR spectra of various PHAs membrane.

3.3.8. Mechanical Properties of Various PHAs Mats

The tensile test is used to provide information on tensile strength, Young's modulus and elasticity of the prepared various PHAs electrospun membranes and cast membranes. Stress-strain curves of these membranes are shown in Fig. 3-11. Table 3-3 summarizes the mechanical properties of different PHAs electrospun membranes or cast membranes. For PHAs electrospun membranes, their Young's modulus and tensile strength increased in the order of PHBV25/PHOHHx (75/25, wt%) < PHBV25 < PHBV12. The same trend was also found on various PHAs cast membranes.

For the same kind of PHA, the mechanical behaviors of electrospun membranes and cast membranes were significantly different.

Young's modulus and tensile strength of electrospun membrane were lower than that of cast membranes. This is due to lower porosity and higher crystallinity of cast membranes when compared with electrospun fibrous membranes. Low Young's modulus is a characteristic property in rubber-like amorphous polymers. Because of the higher HV content, PHBV25 is more amorphous and ductile than PHBV12. By blending PHBV25 with PHOHHx, the most ductile PHAs electrospun membrane was obtained. This is consistent with the crystallinity of various PHAs membranes.

For ideal wound dressings, elasticity and resilience are necessary properties. Elongation at break describes the flexibility or extensibility of the dressings. Tensile strength indicates the capacity of the dressings to resist breaking. Young's modulus specifies the stiffness or rigidity of the dressings[106, 107]. Lee et al.[108] have compared tensile strength and elongation of various commercially available wound dressings, which were in the range of 0.1 ~2.43 MPa and 180~1100%. According to Fetisova and Tsetlin [109], wound dressings should have minimum elongation at break 200%, which corresponds to the natural extensibility of the skin. These values could serve as a benchmark for us to choose which PHA membrane was more suitable for wound dressing applications. Elongation at break of PHBV25 electrospun membrane was slightly higher than 200%, so it was not an ideal application for wound dressing. PHBV25/PHOHHx (75/25, wt%) electrospun membrane had relatively similar tensile strength with respect to that of various commercially available wound dressings, and superior elongation at break (291.32±51.31%), hence it showed potential in wound dressing applications.

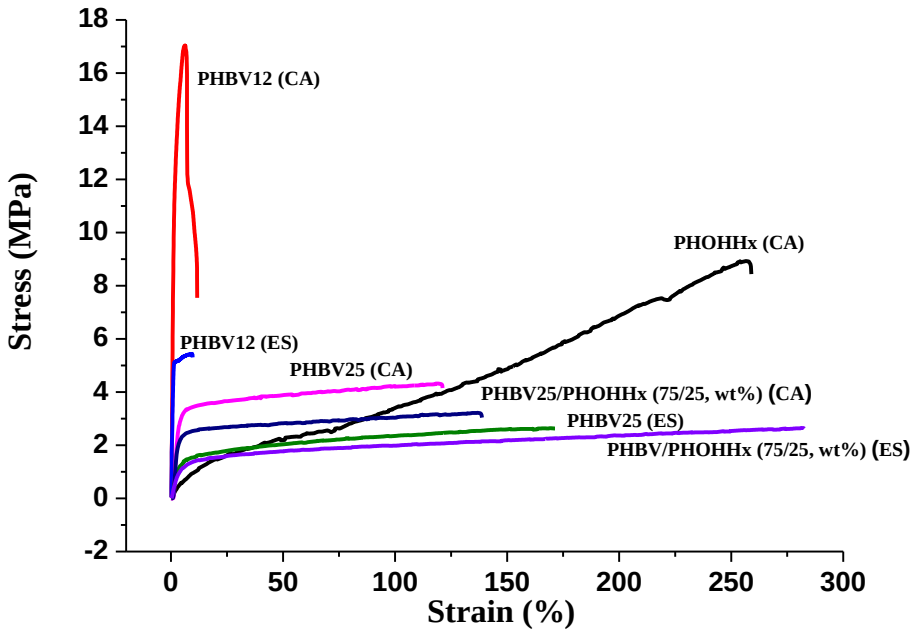

Fig. 3-11. Stress–strain curves of various PHAs membrane. Each curve represents the mean trend after analysis of 5 specimens.

Table 3-3. Mechanical properties of different PHA membranes.

	Young 's modulus (MPa)	Tensile strength (MPa)	Elongation at break (%)
PHOHHx cast membrane	12.54±0.36	9.02±1.7	267.62±25.48
PHBV12 cast membrane	903.29±132.36	18.27±2.09	10.61±1.82
PHBV12 electrospun membrane	547.77±59.71	5.85±0.75	10.20±1.67
PHBV25 cast membrane	136.08±6.32	4.39±0.07	127.6±9.79
PHBV25 electrospun membrane	41.09±3.69	2.90±0.31	212.186±42.22
PHBV25/PHOHHx (75/25, wt%) cast membrane	87.31±8.03	3.67±0.83	138.82±19.24
PHBV25/PHOHHx (75/25, wt%) electrospun membrane	34.46±3.19	2.68±0.05	291.32±51.31

3.4. Conclusion

In this chapter, PHBV25 (scl-PHA) and PHOHHx (mcl-PHA) polymers were blended and used to prepare nanofibrous membranes by electrospinning. PHOHHx alone was non-electrospinnable, but when blended with PHBV25 in the appropriate ratio, nanofibrous mats with good structure were produced. By tuning PHBV25/PHOHHx composition ratios, polymer concentrations, applied voltage, and feeding rate, bead-free and uniform PHAs nanofibers were obtained. With the incorporation of amorphous PHOHHx, both the crystallinity, tensile strength and the Young's modulus of the electrospun nanofiber membrane decreased, while the elongation at break increased. Considering the above-mentioned factors, the blend of PHBV25/PHOHHx (75/25, wt%) nanofibrous membrane should be a promising candidate for wound dressings applications.

4. Bacteria-triggered Release of Potent Biocide from Core-shell PHA Based Nanofibers

4.1. Introduction

In general, nanofibers loaded with antimicrobial agents are prepared by using a mixture of polymer and antimicrobial agent for electrospinning, both of which must be dissolved or finely dispersed in the same solvent. It is observed that during the electrospinning procedure, the antimicrobial agent molecules in the suspension are capable of migrating towards to the nanofiber surface during the process of rapid jet stretching and solvent evaporation of the solution [110, 111]. Thus, a significant burst release in the initial stage of the release test is inevitable. Also, the release kinetics depend on how well the antimicrobial agent is distributed inside the nanofibers. Aside from the aforementioned conventional electrospinning method, there is an alternative way to encapsulate antimicrobial agents inside polymer nanofibers – this can be done using coaxial electrospinning.

Coaxial electrospinning is a technique involving a one-step encapsulation technique to capture antimicrobial agents in polymeric nanofibers. This forms a unique core-shell structure. In general, a shell solution (usually an electrospinnable polymer solution) and core solution (solution containing the antimicrobial agent along with a carrier polymer, which may be electrospinnable) are forced by electrostatic force to eject out through a concentric and multi-channeled spinneret, resulting in core-shell structured nanofibers[110]. Since the antimicrobial agent is restricted to the core layer and protected by the shell layer, the core-shell nanofiber is expected to minimize the amount of antimicrobial agent released in the initial stages of the release test [112].

Poly (ethylene succinate) (PES) (Fig 4-1) is a thermoplastic polyester prepared either by ring-opening copolymerization of succinic anhydride with ethylene oxide or by poly-condensation of succinic acid with ethylene glycol [113]. Similar to PHAs, PES also contains hydrolysable ester bonds in the main chain. The presence of hydrolysable ester bonds makes PES susceptible to lipase hydrolysis. The degree of polyester hydrolysis by lipases increases with decreasing polyester

molecular weight [114]. When compared to the molecular weights of PHBV25 and PHOHHx, which are 180,000 and 98,000, respectively, the molecular weight of PES is only 10,000. This is of importance because by adding PES into a PHBV25/PHOHHx mixture, it can improve the lipase-catalyzed hydrolysis of the polymer blend. Thus, a mixture of PES/PHBV25/PHOHHx should have a higher lipase-catalyzed hydrolysis rate than a mixture of PHBV25/PHOHHx alone. In addition, like PHBV25 and PHOHHx, PES is also a hydrophobic polymer. The addition of PES to PHBV25/PHOHHx will not impair the hydrophobicity of the mixture. Therefore, the hydrophobic tri-component mixture should have a potential to be used as a shell layer material in effectively shielding the inner antimicrobial agent in aqueous solutions.

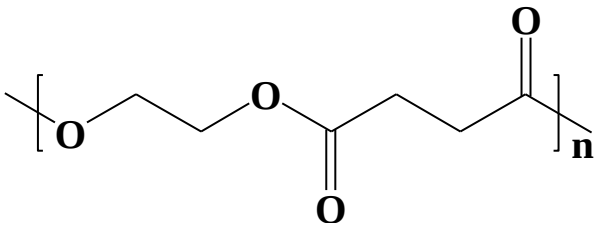

Fig. 4-1. General structure of PES.

Quaternary ammonium compounds (QACs) (Fig 4-2) are amphoteric surfactants that are widely used as antimicrobial agents in clinical and industrial environments[115]. Surfactant properties and potent broad-spectrum antimicrobial activities have made QACs the most commonly used cationic antimicrobials, as well as the most ideal antimicrobials for wound care management [116]. The antimicrobial action of QACs involves long chain length QAC binding to microbial membrane surfaces by ionic and hydrophobic interactions. Hydrophobic tails that can be found on the side chains then enter the lipid bilayer of bacteria, causing rearrangement of the bacterial membrane and subsequent leakage of intracellular constituents. This subjects the bacterial cells to lysis.

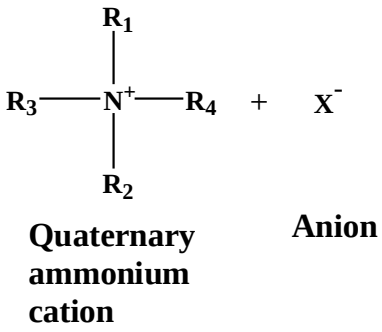

Fig. 4-2. A general structure of a quaternary ammonium compound.

Herein, I report a new approach to achieve an on-demand release (bacteria lipase response release) of biocide from wound dressings. Unique core-shell structure nanofibers were fabricated with the method of coaxial electrospinning. Single nanofibers prepared by conventional electrospinning mixture of DTAC and PHBV25/PHOHHx/PES were used as control. Dodecyltrimethylammonium chloride (DTAC, a type of QAC) (Fig 4-3) and carrier polymer polyvinylpyrrolidone (PVP) were chosen as the core layer.

A PHBV25/PHOHHx/PES blend was chosen as the shell layer. The hydrophobic PHBV25/PHOHHx/PES shell can effectively prevent the biocide from an undesirable payload release in physiological environments, without the stimulation of bacterial lipase. However, in the presence of bacterial lipase, the PHBV25/PHOHHx/PES shell could be hydrolysed by lipase, and the encapsulated biocide could be released. The released biocide subsequently could impose targeted antimicrobial effects on the bacteria.

The morphology of core-shell nanofibers was confirmed using scanning electron microscope (SEM) imaging. Core-shell nanofibers showed lower cumulative release than single nanofibers, owing to the preservation of the PHBV25/PHOHHx/PES shell. A higher cumulative release was observed in the bacterial supernatant than in PBS due to the presence of lipase in bacterial supernatant. Single nanofibers and core-shell nanofibers reduced *Pseudomonas aeruginosa*

bacterial growth by 97.4% and 86.9%, respectively, after 2 h of culturing, and then to 98.9% and 98%, respectively, after 4 h of culturing.

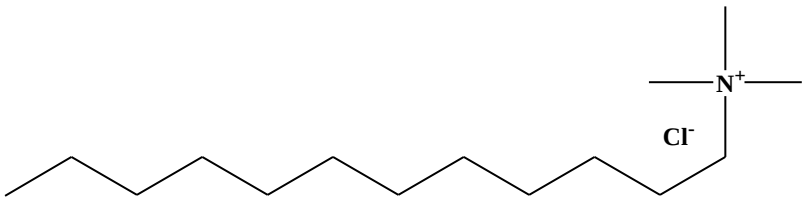

Fig. 4-3. Chemical structure of dodecyltrimethylammonium chloride (DTAC).

4.2. Materials and methods

4.2.1. Materials

PHBV 25 (with HV content of 25 mol %) was produced by *Ralstonia eutropha* H16 on the substrate of waste oil supplemented with valeric acid. PHOHHx (with HO content of 92.6 mol % and HHx content of 6.1 mol%) was produced by *Pseudomonas putida* LS46 on the substrate of octanoic acid. PHA was purified before use. Briefly, the purification was performed by dissolving PHA in chloroform followed by precipitation in methanol and filtration. Polyvinylpyrrolidone (PVP, Mw=40,000), Luria-Bertani (LB) broth, chloroform ($CHCl_3$), dimethyl formamide (DMF) and orange ii sodium salt (a model dye for *in vitro* release test) were purchased from Sigma-Aldrich, Canada. Poly (ethylene succinate) (PES) (Mw=10,000) was purchased from Scientific Polymer Products, Inc. Dodecyltrimethylammonium chloride (DTAC), a kind of quaternary ammonium compound, was purchased from Alfa Aesar. *Pseudomonas aeruginosa* PA01 was used as model bacteria for antimicrobial test.

4.2.2. Single nozzle electrospinning process

PHBV25/PES/PHOHHx in a ratio of 3:2:1 (w/w) were dissolved in mixture of chloroform/DMF (80/20 vol%) with sufficient stirring at the concentration of 24% (w/v). Then 1.5% of model drug (DTAC) or model dye (orange ii sodium salt) with respect to the weight of whole

polymer was added to prepare a final solution for single nozzle electrospinning, or conventional electropsinning. The final solution was loaded into a plastic syringe (6 mL) which was connected to the single channel spinneret. The flow rate of solution was fixed at 1 mL/h. The applied voltage was kept between 14 and 16 kV with a tip-to-collector distance at 17 cm. The nanofibers, termed as single nanofibers, were collected on a ground plate collector (diameter of 10 cm). As spun mat was carefully detached from the collector and placed in vacuum oven for 48 h at room temperature to remove residual solvents.

4.2.3. Coaxial electrospinning process

PHBV25/PES/PHOHHx=3:2:1 (w/w) was dissolved in chloroform/DMF (80/20 vol%) with sufficient stirring at the concentration of 24% (w/v) as shell solution. To prepare core solution of DTAC/PVP (or orange ii sodium salt/PVP), DTAC (or orange ii sodium salt) was first dissolved in chloroform/DMF (80/20 vol%), followed by addition of PVP at the concentration of 20% (w/v). 1.5% of DTAC (or orange ii sodium salt) with respect to the weight of whole polymer was used to study the antibacterial efficacy (or in vitro release) of nanofibers. Shell and core solutions were loaded in two individual 6 mL syringes separately which were connected to the coaxial spinneret. The flow rates of shell and core solutions were fixed at 1 mL/h and 0.2 mL/h, respectively. The applied voltage was kept between 14 and 16 kV with a tip-to-collector distance of 17 cm. The core-shell nanofibers were collected on a grounded plate collector (diameter of 10 cm). Electrospun mats were carefully detached from the collector and dried in vacuum oven at room temperature for 48 h to remove residue solvent.

4.2.4. Morphology of as-spun nanofibrous mats

Coaxial electrospun mat was firstly immersed in distilled water for 2 minutes. And then the wet mat was placed in liquid nitrogen until brittle and was split into pieces. These split pieces were immersed in distilled water for 5 hours to completely dissolve the core layer polymer PVP. The

hollow structure nanofibers could be confirmed from the cross sectional view of the split mats. The morphological appearance of the as-spun nanofibers (both top view and cross sectional view) was observed with a FEI environmental scanning electron microscope (Quanta 650 FEG) after sputter-coated with gold for 30 s. The average diameter and the diameter distribution were measured by Image J software from SEM pictures with the average value being calculated from at least 100 measurements.

4.2.5. Mechanical tests

Mechanical properties in terms of tensile strength, Young's modulus, and elongation at break were measured by using an Instron tester (3366 dual column tabletop testing system). The dimensions of samples with dimensions of 40 mm × 5 mm were cut out from electrospun mats. The apparent thickness of the membranes was determined by a digital vernier caliper. The apparent thickness was in the range of ~ 0.1 mm to 0.3 mm. Samples were fixed with two clamps in a vertical position and preloaded at 0.01 N. After the preloading, the force was set to zero and a constant crosshead speed of 10 mm/min was determined. Data were collected until the sample's rupture. Strain-stress curves were recorded. Computer software NEXYGEN PLUS provided the tensile strength (MPa), the percentage elongation at the break moment (%) and Young's modulus (MPa). Five independent replicated experiments were conducted for each condition tested, and the results were expressed as the means ± standard error.

4.2.6. *In vitro* release experiments

In vitro release experiments were conducted in phosphate buffered saline (PBS) and cell-free bacteria supernatant. Initially *Pseudomonas aeruginosa* PA01 (wild type) colonies were suspended in PBS at a density equivalent to 0.5 McFarland standard of $1*10^8$ CFU/mL, and then diluted 100 times to $1*10^6$ CFU/mL. 15μL of diluted *P. aeruginosa* suspension was further diluted into 45 mL LB broth. After culturing in the incubator at 37°C for 18 hours (h), the concentration of bacteria

went up to 10^8 CFU/mL again. After centrifugation (5000 rpm for 15 min) and filter-sterilization (0.22 μm filters), cell-free bacteria supernatant was prepared. For *in vitro* release tests, orange ii sodium salt (Fig 4-4) was chosen as a replacement for biocide and was encapsulated within the nanofibers (both single nanofibers and coaxial electrospun nanofibers).

To evaluate the cumulative release of orange ii sodium salt in PBS and cell-free bacteria supernatant, both conventional and coaxial electrospun mats were cut into small rectangular pieces (size of 10*10 mm^2, and mass of 13 mg). These small pieces were immersed in 8 mL of PBS (pH 7.4) or cell-free bacteria supernatant (pH 7.12) at 37 °C. At predetermined time intervals, 500 μL of eluted orange ii sodium salt medium was removed for quantification and same volume of fresh medium was replenished for continuing incubation. The amount of orange ii sodium salt released in the medium was determined by a Biotek Powerwave XS2 microplate reader (λab = 483 nm). The results were presented in terms of cumulative release as a function of release time:

Cumulative amount of release, $\% = \frac{M_t}{M_\infty} \times 100$ (4-1)

where Mt is the amount of released orange ii sodium salt at time t and M∞ is the total amount of orange ii sodium salt loaded in the nanofibrous membranes. All samples were run in triplicate.

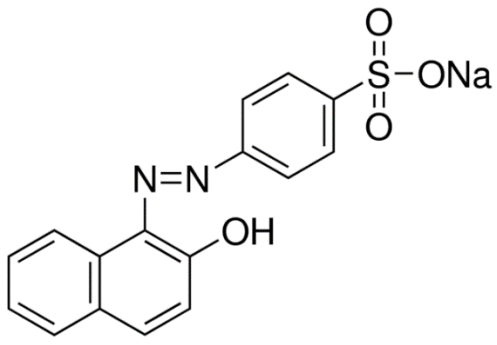

Fig 4-4. Chemical structure of orange ii sodium salt.

4.2.7. Antimicrobial activity evaluation

The antimicrobial activity of the DTAC-free mat and DTAC-loaded mats (both conventional and coaxial electrospun mats) was quantitatively evaluated by a colony counting method using *Pseudomonas aeruginosa* PA01 as the model bacteria. Log phase cultures were prepared by initially suspending several *P. aeruginosa* colonies in PBS at a density equivalent to 0.5 McFarland standard of 1*10^8 CFU/mL and then diluted 100 times. 15 μL of diluted *P. aeruginosa* PA01 was further diluted into 45 mL Luria-Bertani (LB) broth and incubated at 37°C for 18 hours. The finial suspension (3.0*10^8) was used for assaying.

The mat (size of 10*10 mm^2, and mass of 13 mg) was immersed into a bacteria suspension (3 mL) and kept in incubator at 37 °C for 2 h and 4 h. At each time interval, a CFU counting method was used to estimate the number of viable *P. aeruginosa* remaining in the suspension. From the bacteria suspension, 30 μL was serially diluted and 50 μL diluted suspension was pipetted into freshly prepared LB agar plates. The LB agar plates were incubated at 37°C overnight and the developed bacteria colonies were counted. The antimicrobial efficiency was calculated using Eq. (4-2):

$$\text{Antimicrobial efficiency (\%)}=\frac{CFU_{(control)}-CFU_{(sample)}}{CFU_{(control)}}\times 100\% \quad (4\text{-}2)$$

A control group was taken as the bacteria inoculation without any membrane. Before experiments, all electrospun mat samples were sterilized with UV irradiation and all glassware and plastic were sterilized by autoclaving.

4.3. Results and discussion

4.3.1. Coaxial electrospinning

The main idea of this study was to fabricate core-shell structure nanofibrous mats by using coaxial electrospinning technique in which PVP/DTAC was used for the core layer and tri-

component mixture PHBV25/PES/PHOHHx (3:2:1, w/w) was used for the shell layer, which doesn't exist in the literature. A digital image of the coaxial electrospinning setup is shown in Fig 4-5. The concentric spinneret for coaxial electrospinning is shown in the insert of Fig 4-5. Shell solution and inner solution were loaded in separate syringes and driven by corresponding syringe pumps. The process of coaxial electrospinning is similar to that of conventional electrospinning. When polymer solutions are charged at high voltage, the surface charge accumulation mainly occurs on the shell solution coming out of the concentric spinneret. Then a Taylor cone is formed due to the electrostatic repulsion. As the electrostatic repulsion outweighs surface tension, the shell polymer solution is ejected to the plate collector. Meanwhile, the core solution is also carried within the shell solution by the shear stress generated at the interface between shell and core solutions, hence the formation of core-shell structure nanofibers.

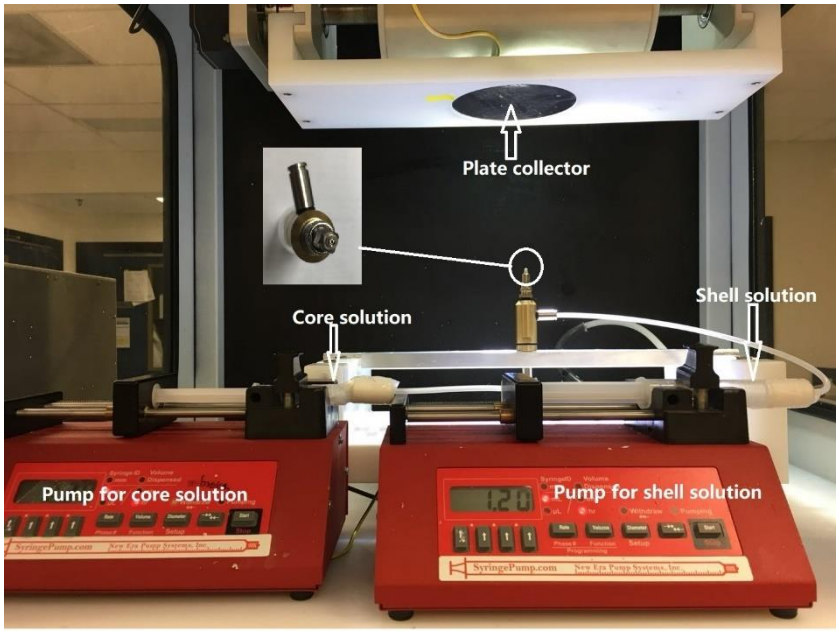

Fig 4-5. Coaxial electrospinning: digital image showing the arrangement of apparatus (the inset is a photo of the concentric spinneret).

4.3.2. Morphology of coaxial electrospun nanofibers

As mentioned in the introduction section, coaxial electrospun nanofibers provide benefits over conventional electrospun nanofibers (single nanofibers). Since biocide DTAC is restricted to the core layer, the hydrophobic polyester shell is expected to minimize the amount of biocide released in the initial stages. The core layer is made of PVP and DTAC, which are both water soluble; while the shell layer is made of PHAs and PES, which are insoluble in water. To confirm the core-shell structure nanofibers, the coaxial electrospun mat was firstly immersed in distilled water for 2 minutes, then the wet mat was immersed in liquid nitrogen for a few minutes until it became brittle. The brittle mat was split into several small pieces in liquid nitrogen, so the core-shell structure of nanofibers on the newly-created side was maintained intact. The split pieces were immersed in distilled water again for 5 h to completely dissolve the inner layer. Hence, only the shell layer was left, and the nanofibers were hollow.

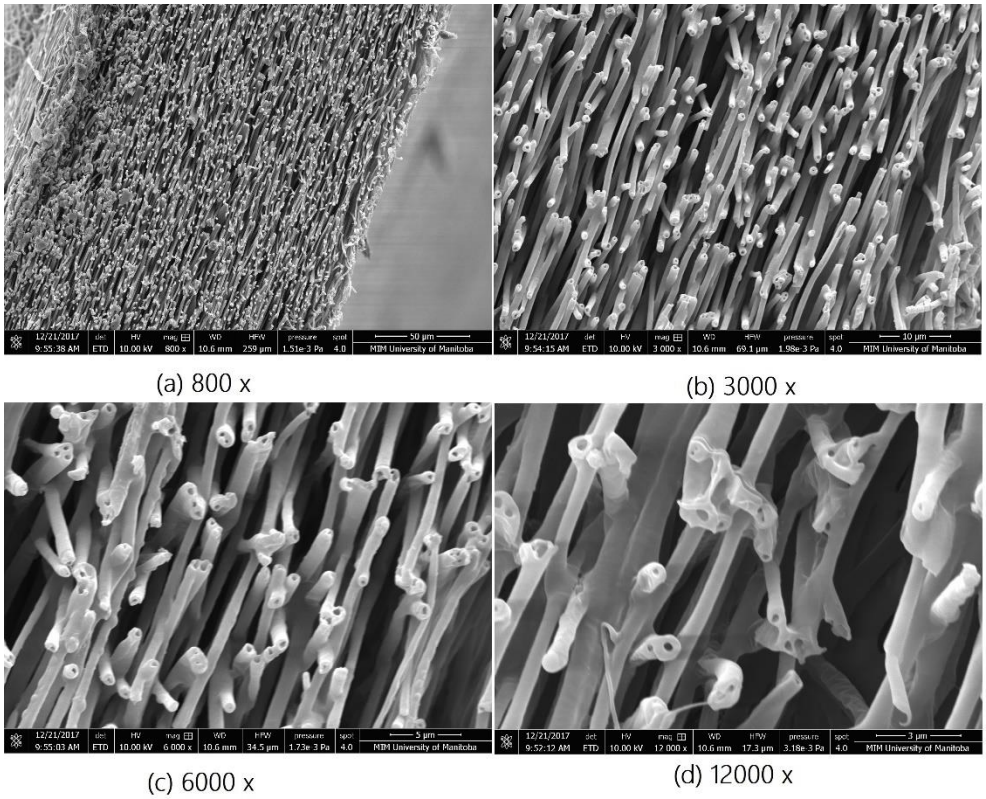

Fig 4-6. Cross-sectional morphology of coaxial electrospun nanofibers. Immersed in water for 5 hours following cracking in liquid nitrogen.

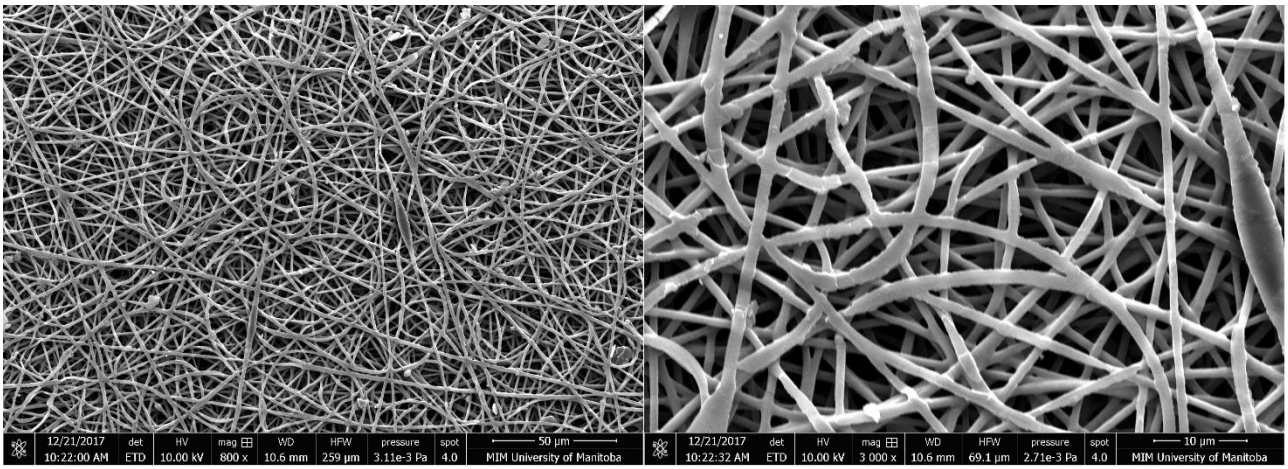

Fig 4-7. Top view morphology of coaxial electrospun nanofibers.

As shown in Fig 4-6, the cross-sectional morphology of hollow nanofibers was observed. From the top view, Fig 4-7 shows coaxial electrospun nanofibers had morphology with smooth surface and uniform structure. It confirmed that biocide DTAC was homogeneously distributed within the nanofibers. The average size of holes (in Fig 4-6) was 286.4±98.4 nm, while the average diameter of the core-shell structure nanofibers was 672.9±87.5 nm.

4.3.3. Mechanical properties of coaxial electrospun mats

In order to achieve a successful wound dressing, two properties are necessary: elasticity and resiliency. Elongation at break describes the flexibility or extensibility of the dressings. Tensile strength indicates the capacity of the dressings to resist breaking. Young's modulus specifies the stiffness or rigidity of the dressings [106, 107]. In Chapter 3, PHBV25/PHOHHx (75/25, wt%) conventional electrospun mat has shown superior mechanical properties for wound dressing application. In order to enhance the shell enzymatic hydrolysis and realize faster lipase response, low molecular weight PES (Mw=10,000) was blended with PHBV25/PHOHHx for coaxial electrospinning, whereas the molecular weight of PHBV25 and PHOHHx were 180,000 and 98,000, respectively. After trials of a series of ratios, PHBV25/PES/PHOHHx with ratio of 3:2:1 (w/w) was finally selected for the shell layer. The mechanical properties of coaxial electrospun PHBV25/PES/PHOHHx mats were compared with conventional electrospun PHBV25/PHOHHx mats. Tensile strength, elongation at break and Young's modulus of PHBV25/PES/PHOHHx coaxial electrospun mats and PHBV25/PHOHHx conventional electrospun mats are listed in Table 4-1. Stress-strain curves of these mats are shown in Fig 4-8. As shown in Fig 4-8 and Table 4-1, the tensile strength and Young's modulus of PHBV25/PES/PHOHHx coaxial electrospun mats were significantly lower than those of PHBV25/PHOHHx mats. The presence of low molecular weight PES weakens the strength of mats. Also, as PES was mixed with PHBV25/PHOHHx, the ductility of mat decreased.

Table 4-1. Mechanical properties of PHA/PES coaxial electrospun mats and PHBV25/PHOHHx single electrospun mats.

	Young 's modulus (MPa)	Tensile strength (MPa)	Elongation at break (%)
PHA/PES coaxial electrospun	25.56±2.60	0.96±0.15	133.38±15.30
PHBV/PHOHHx single electrospun	34.46±3.19	2.68±0.05	291.32±51.31

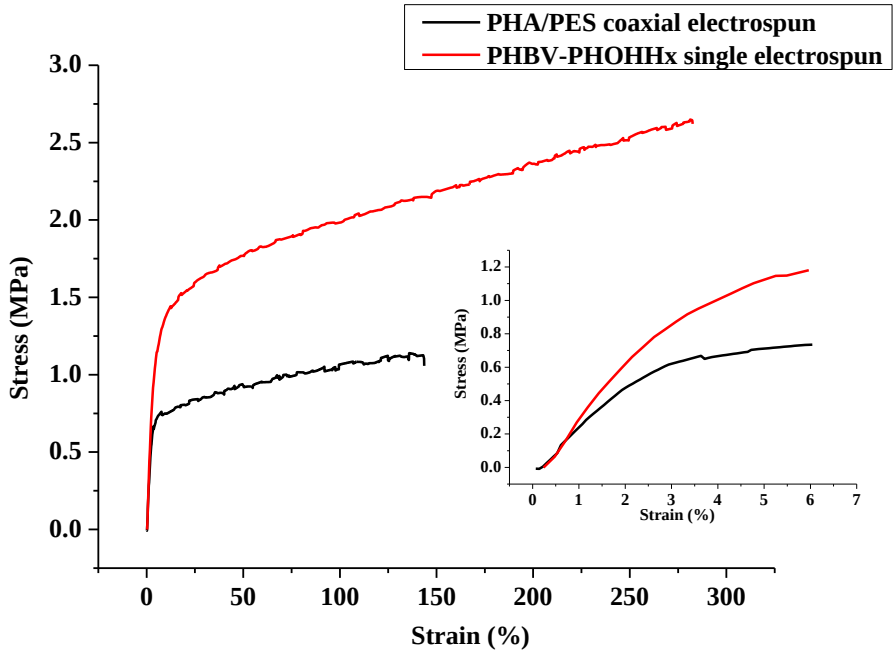

Fig 4-8. Stress–strain curves of PHA/PES coaxial electrospun mats and PHBV25/PHOHHx. single electrospun mats.

4.3.4. *In vitro* release profile

Dodecyltrimethylammonium chloride (DTAC) is a quaternary ammonium compound (QAC) commonly used as an antimicrobial and disinfectant. Long chain length QACs bind to microbial membrane surfaces by ionic and hydrophobic interactions. Then the hydrophobic tails insert into the lipid bilayer of bacteria, causing the rearrangement of the bacteria membrane and subsequent

leakage of intracellular constituents. Since DTAC is an aliphatic QAC, which doesn't show any UV absorbance, orange ii sodium salt was used as a model dye to study biocide in vitro release kinetics. Release performance differences between model dye loaded single and coaxial electrospun nanofibers in both PBS and cell-free supernatant during 72 h were plotted in Fig 4-9. The experiments were performed in triplicate to obtain more accurate results. The experimental results were the average of triplicate measurements.

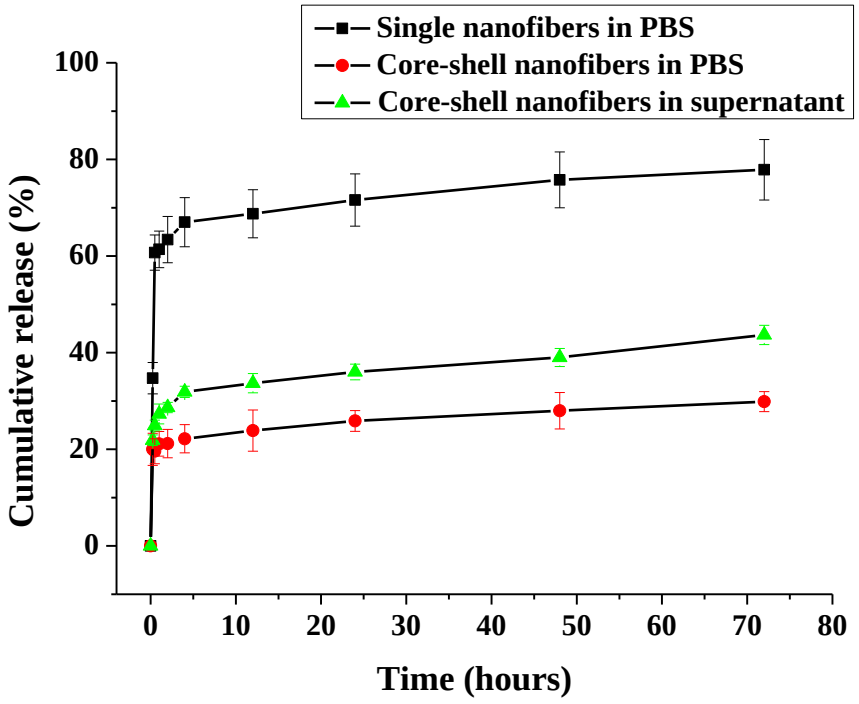

Fig 4-9. Cumulative release of orange ii sodium salt from single nanofibers and core-shell nanofibers in PBS and cell-free supernatant

The release behavior of orange ii sodium salt can be illustrated by two stages: an initial burst release followed by a slow release. The burst release was around 60% for single nanofibers and around 20% for coaxial electrospun nanofibers. Single nanofibers showed higher burst release than coaxial electrospun nanofibers because most of the dye molecules were localized on the surface of

nanofibers during electrospinning process[117]. As the whipping jet moved towards the plate collector, solvents in the jet evaporated quickly. As a result, the dye molecules migrated from the inner part to surface layer. The slow orange ii sodium salt release rate of coaxial electrospun nanofibers in PBS is due to the restriction of dye in the core layer of nanofibers which postpones the diffusion of it. In addition, coaxial electrospun nanofibers showed a higher release rate in cell-free supernatant (40%) than in PBS (25%), because of the extracellular lipases presence in the cell-free supernatant. Lipases can be involved in the hydrolysis of esters[118], and *P. aeruginosa* has been reported to be able to secrete extracellular lipase into culture medium [80]. *P. aeruginosa* triggered higher amounts of payload released from core-shell nanofibers by enzymatic degradation of ester linkage in shell part of nanofibers.

4.3.5. Antimicrobial test

The aim of the present study was to design an antimicrobial wound dressing. Among different potential biocides, DTAC was chosen in the present work as payload. Antimicrobial properties of DTAC-loaded and DTAC-free mats were quantitatively evaluated by a colony counting method using *P. aeruginosa* PA01 as model bacteria, which can cause skin and soft tissues infection.

When DTAC-free mat was cultured with *Pseudomonas aeruginosa*, no reduction in bacterial cells was observed. DTAC-loaded single electrospun and coaxial electrospun nanofibrous mats reduced *Pseudomonas aeruginosa* bacterial growth after 2 h of culturing by 97.4% and 86.9%, respectively. As we expected, coaxial electrospun nanofibrous mat showed less bacteria inhibition than single electrospun nanofibrous mat, which is consistent with the release data. Hydrophobic nature of the shell (PHAs and PES) could effectively retard the penetration of water into the nanofibers and thereby reduce the release DTAC within 2 h. After 4 h of culture, bacterial growth reduced by 98.9% and 98%, respectively. According to this result, antimicrobial activity of the coaxial electrospun mat progressively increased as the contact time increased, while that of single

electrospun mat didn't show a significant increase. This is consistent with the data of in vitro release: 60% of biocide loaded in single electrospun mat was released within 2 h, and it only increased to 65% within 4 h. The coaxial electrospun mat showed a prolonged and efficient antibacterial properties.

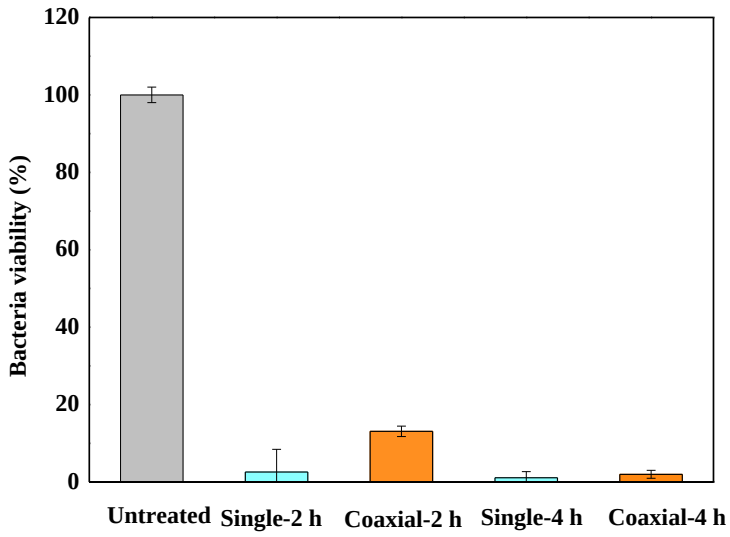

Fig 4-10. Bacteria viability at various contact times (2 h and 4 h) at 37 °C.

4.3.6. Conclusions

In this portion of research, a coaxial electrospinning technique was used to fabricate polymeric nanofibers with a core-shell structure. PHBV25/PHOHHx/PES was chosen as the shell layer, while the broad-spectrum potent biocide DTAC and carrier polymer PVP were chosen as the core layer. Core-shell structure of nanofibers was confirmed using scanning electron microscope (SEM) imaging. When compared with conventional electrospun nanofibers (single nanofibers), lower burst release of the biocide (DTAC) was observed on core-shell nanofibers owing to the preservation of PHBV25/PHOHHx/PES shell. Cumulative release of biocide was higher in supernatant than in PBS solution, which was attributed to the presence of lipase in supernatant.

Single nanofibers and core-shell nanofibers reduced *P. aeruginosa* bacterial growth by 97.4% and 86.9%, respectively, after 2 h of culturing, and then to 98.9% and 98%, respectively, after 4 h of culturing. Due to these properties of the bacteria responsive PHA-based electrospun nanofibrous mat, it provides a smart, safe and effective approach for the treatment of topical wound infections.

5. Future work and recommendation

Bacteria triggered release of biocide has been confirmed from the PHA-based core-shell nanofibrous mat. But the burst release in the initial stages is still more than 20% even in PBS. The top priority of the future work is to decrease the biocide initial burst release, which may be attributed to diffusion of the small molecular biocide to the shell layer caused by a possible mix of the sheath solvents (chloroform/DMF,80/20 vol%) with the core solvents (chloroform/DMF,80/20 vol%) at the tip of the coaxial spinneret during the coaxial electrospinning process. By eliminating core and shell solvent mixing, different solvents can be used for core and shell solutions in future work. Also, the degradation rate of shell by bacteria lipase should also be increased by choosing lower molecular weight PHAs. Polyester molecular weight has a significant impact on degradation rate by lipase. Finally, cytotoxicity of biocide loaded PHA-based core-shell nanofibrous mat should be evaluated against human fibroblast cells. An ideal wound dressing should not release toxic products or produce adverse effects.

6. References

[1] E. Mele, Electrospinning of natural polymers for advanced wound care: towards responsive and adaptive dressings, J. Mater. Chem. B 4(28) (2016) 4801-4812.

[2] M. Abrigo, S.L. McArthur, P. Kingshott, Electrospun Nanofibers as Dressings for Chronic Wound Care: Advances, Challenges, and Future Prospects, Macromol. Biosci. 14(6) (2014) 772-792.

[3] J. Gerardo-Nava, T. Führmann, K. Klinkhammer, N. Seiler, J. Mey, D. Klee, M. Möller, P.D. Dalton, G.A. Brook, Human neural cell interactions with orientated electrospun nanofibers in vitro, Nanomedicine 4(1) (2008) 11-30.

[4] T. Subbiah, G.S. Bhat, R.W. Tock, S. Parameswaran, S.S. Ramkumar, Electrospinning of nanofibers, J. Appl. Polym. Sci. 96(2) (2005) 557-569.

[5] S. Agarwal, J.H. Wendorff, A. Greiner, Progress in the field of electrospinning for tissue engineering applications, Adv. Mater. 21(32-33) (2009) 3343-3351.

[6] L. Susan, L. Bojun, M. Zuwei, W. He, C. Casey, R. Seeram, Biomimetic electrospun nanofibers for tissue regeneration, Biomed. Mater. 1(3) (2006) 45-53.

[7] Z. Huang, Y.Z. Zhang, M. Kotaki, S. Ramakrishna, A review on polymer nanofibers by electrospinning and their applications in nanocomposites, Compos. Sci. Technol. 63(15) (2003) 2223-2253.

[8] Q.P. Pham, U. Sharma, A.G. Mikos, Electrospinning of polymeric nanofibers for tissue engineering applications: a review, Tissue Eng. 12(5) (2006) 1197-1211.

[9] W. Li, N. Cicek, D.B. Levin, S. Liu, Enabling electrospinning of medium-chain length polyhydroxyalkanoates (PHAs) by blending with short-chain length PHAs, Int. J. Polym. Mater. Po (2018) 1-11.

[10] S. Torres-Giner, R. Pérez-Masiá, J.M. Lagaron, A review on electrospun polymer nanostructures as advanced bioactive platforms, Polymer Engineering & Science 56(5) (2016) 500-527.

[11] Muhammadi, Shabina, M. Afzal, S. Hameed, Bacterial polyhydroxyalkanoates-eco-friendly next generation plastic: production, biocompatibility, biodegradation, physical properties and applications, Green. Chem. Lett. Rev. 8(3-4) (2015) 56-77.

[12] K.P. Luef, F. Stelzer, F. Wiesbrock, Poly(hydroxy alkanoate)s in medical applications, Chem. Biochem. Eng. Q. 29(2) (2015) 287-297.

[13] A. Toncheva, M. Spasova, D. Paneva, N. Manolova, I. Rashkov, Polylactide (PLA)-based electrospun fibrous materials containing ionic drugs as wound dressing materials: a review, Int. J. Polymer. Mater. 63(13) (2014) 657-671.

[14] I. Cantón, R. McKean, M. Charnley, K.A. Blackwood, C. Fiorica, A.J. Ryan, S. MacNeil, Development of an Ibuprofen-releasing biodegradable PLA/PGA electrospun scaffold for tissue regeneration, Biotechnol. Bioeng. 105(2) (2010) 396-408.

[15] O. Suwantong, Biomedical applications of electrospun polycaprolactone fiber mats, Polym. Adv. Technol. 27(10) (2016) 1264-1273.

[16] J.M. Anderson, M.S. Shive, Biodegradation and biocompatibility of PLA and PLGA microspheres, Adv. Drug Del. Rev. 64, Supplement (2012) 72-82.

[17] M.S. Taylor, A.U. Daniels, K.P. Andriano, J. Heller, Six bioabsorbable polymers: In vitro acute toxicity of accumulated degradation products, J. Appl. Biomater. 5(2) (1994) 151-157.

[18] G.E. Luckachan, C.K.S. Pillai, Biodegradable polymers- a review on recent trends and emerging perspectives, J. Polym. Environ. 19(3) (2011) 637-676.

[19] C.M. Agrawal, K.A. Athanasiou, Technique to control pH in vicinity of biodegrading PLA-PGA implants, J Biomed Mater Res 38(2) (1997) 105-14.

[20] K.-E. Jaeger, S. Ransac, B.W. Dijkstra, C. Colson, M. van Heuvel, O. Misset, Bacterial lipases, FEMS Microbiol. Rev. 15(1) (1994) 29-63.

[21] V.V. Komnatnyy, W.-C. Chiang, T. Tolker-Nielsen, M. Givskov, T.E. Nielsen, Bacteria-Triggered Release of Antimicrobial Agents, Angew. Chem. 126(2) (2014) 449-451.

[22] M. Lemoigne, Produits de dehydration et de polymerisation de l'acide ß-oxobutyrique, Bull. Soc. Chim. Biol. (Paris) 8 (1926) 13.

[23] C.S.K. Reddy, R. Ghai, Rashmi, V.C. Kalia, Polyhydroxyalkanoates: an overview, Bioresour. Technol. 87(2) (2003) 137-146.

[24] E. Bugnicourt, P. Cinelli, A. Lazzeri, V.A. Alvarez, Polyhydroxyalkanoate (PHA): Review of synthesis, characteristics, processing and potential applications in packaging, Express Polymer Letters 8(11) (2014) 791-808.

[25] F. Masood, T. Yasin, A. Hameed, Polyhydroxyalkanoates – what are the uses? Current challenges and perspectives, Crit. Rev. Biotechnol. 35(4) (2015) 514-521.

[26] R. Rai, T. Keshavarz, J.A. Roether, A.R. Boccaccini, I. Roy, Medium chain length polyhydroxyalkanoates, promising new biomedical materials for the future, Mater. Sci. Eng. R. Rep. 72(3) (2011) 29-47.

[27] T.R. Heathman, W.R. Webb, J. Han, Z. Dan, G.Q. Chen, N.R. Forsyth, A.J. El Haj, Z.R. Zhang, X. Sun, Controlled production of poly (3-hydroxybutyrate-co-3-hydroxyhexanoate)(PHBHHx) nanoparticles for targeted and sustained drug delivery, J. Pharm. Sci. 103(8) (2014) 2498-2508.

[28] D.P. Martin, S.F. Williams, Medical applications of poly-4-hydroxybutyrate: a strong flexible absorbable biomaterial, Biochem. Eng. J. 16(2) (2003) 97-105.

[29] D.F. Williams, On the mechanisms of biocompatibility, Biomaterials 29(20) (2008) 2941-2953.

[30] C.J. Brigham, A.J. Sinskey, Applications of Polyhydroxyalkanoates in the Medical Industry, Int. J. Biotech. Well. Indus. 1(1) (2012) 52-60.

[31] E.I. Shishatskaya, T.G. Volova, A comparative investigation of biodegradable polyhydroxyalkanoate films as matrices for in vitro cell cultures, J. Mater. Sci. Mater. Med. 15(8) (2004) 915-923.

[32] S.K. Misra, S.P. Valappil, I. Roy, A.R. Boccaccini, Polyhydroxyalkanoate (PHA)/Inorganic Phase Composites for Tissue Engineering Applications, Biomacromolecules 7(8) (2006) 2249-2258.

[33] K. Zhao, Y. Deng, J. Chun Chen, G.-Q. Chen, Polyhydroxyalkanoate (PHA) scaffolds with good mechanical properties and biocompatibility, Biomaterials 24(6) (2003) 1041-1045.

[34] S.P. Valappil, S.K. Misra, A.R. Boccaccini, I. Roy, Biomedical applications of polyhydroxyalkanoates, an overview of animal testing and in vivo responses, Expert Rev. Med. Devices 3(6) (2006) 853-868.

[35] C. Yan, Y. Wang, X.-Y. Shen, G. Yang, J. Jian, H.-S. Wang, G.-Q. Chen, Q. Wu, MicroRNA regulation associated chondrogenesis of mouse MSCs grown on polyhydroxyalkanoates, Biomaterials 32(27) (2011) 6435-6444.

[36] G.T. Köse, F. Korkusuz, P. Korkusuz, N. Purali, A. Özkul, V. Hasırcı, Bone generation on PHBV matrices: an in vitro study, Biomaterials 24(27) (2003) 4999-5007.

[37] S.V. Naveen, I.K.P. Tan, Y.S. Goh, H.R. Balaji Raghavendran, M.R. Murali, T. Kamarul, Unmodified medium chain length polyhydroxyalkanoate (uMCL-PHA) as a thin film for tissue engineering application – characterization and in vitro biocompatibility, Mater. Lett. 141 (2015) 55-58.

[38] Q. Wu, Y. Wang, G.-Q. Chen, Medical Application of Microbial Biopolyesters Polyhydroxyalkanoates, Artificial Cells, Blood Substitutes, and Biotechnology 37(1) (2009) 1-12.

[39] X.-H. Qu, Q. Wu, K.-Y. Zhang, G.Q. Chen, In vivo studies of poly(3-hydroxybutyrate-co-3-hydroxyhexanoate) based polymers: Biodegradation and tissue reactions, Biomaterials 27(19) (2006) 3540-3548.

[40] C. Kunze, H. Edgar Bernd, R. Androsch, C. Nischan, T. Freier, S. Kramer, B. Kramp, K.-P. Schmitz, In vitro and in vivo studies on blends of isotactic and atactic poly (3-hydroxybutyrate) for development of a dura substitute material, Biomaterials 27(2) (2006) 192-201.

[41] T. Freier, C. Kunze, C. Nischan, S. Kramer, K. Sternberg, M. Saß, U.T. Hopt, K.-P. Schmitz, In vitro and in vivo degradation studies for development of a biodegradable patch based on poly(3-hydroxybutyrate), Biomaterials 23(13) (2002) 2649-2657.

[42] S. Gogolewski, M. Jovanovic, S.M. Perren, J.G. Dillon, M.K. Hughes, Tissue response and in vivo degradation of selected polyhydroxyacids: Polylactides (PLA), poly(3-hydroxybutyrate) (PHB), and poly(3-hydroxybutyrate-co-3-hydroxyvalerate) (PHB/VA), J. Biomed. Mater. Res. 27(9) (1993) 1135-1148.

[43] A. Hazari, M. Wiberg, G. Johansson-Rudén, C. Green, G. Terenghi, A resorbable nerve conduit as an alternative to nerve autograft in nerve gap repair, Br. J. Plast. Surg. 52(8) (1999) 653-657.

[44] E.I. Shishatskaya, T.G. Volova, S.A. Gordeev, A.P. Puzyr, Degradation of P(3HB) and P(3HB-co-3HV) in biological media, J. Biomater. Sci. Polym. Ed. 16(5) (2005) 643-657.

[45] N.D. Miller, D.F. Williams, On the biodegradation of poly-β-hydroxybutyrate (PHB) homopolymer and poly-β-hydroxybutyrate-hydroxyvalerate copolymers, Biomaterials 8(2) (1987) 129-137.

[46] T. Saito, K. Tomita, K. Juni, K. Ooba, In vivo and in vitro degradation of poly(3-hydroxybutyrate) in pat, Biomaterials 12(3) (1991) 309-312.

[47] L.S. Nair, C.T. Laurencin, Biodegradable polymers as biomaterials, Prog. Polym. Sci. 32(8–9) (2007) 762-798.

[48] L. Kostopoulos, T. Karring, Guided bone regeneration in mandibular defects in rats using a bioresorbable polymer, Clin. Oral Implants Res. 5(2) (1994) 66-74.

[49] Z.B. Luklinska, W. Bonfield, Morphology and ultrastructure of the interface between hydroxyapatite-polyhydroxybutyrate composite implant and bone, J. Mater. Sci. Mater. Med. 8(6) (1997) 379-383.

[50] S. Philip, T. Keshavarz, I. Roy, Polyhydroxyalkanoates: biodegradable polymers with a range of applications, J. Chem. Technol. Biotechnol. 82(3) (2007) 233-247.

[51] A. Rogina, Electrospinning process: versatile preparation method for biodegradable and natural polymers and biocomposite systems applied in tissue engineering and drug delivery, Appl. Surf. Sci. 296 (2014) 221-230.

[52] Z. Sun, E. Zussman, A.L. Yarin, J.H. Wendorff, A. Greiner, Compound Core–Shell Polymer Nanofibers by Co-Electrospinning, Adv. Mater. 15(22) (2003) 1929-1932.

[53] O. Suwantong, S. Waleetorncheepsawat, N. Sanchavanakit, P. Pavasant, P. Cheepsunthorn, T. Bunaprasert, P. Supaphol, In vitro biocompatibility of electrospun poly(3-hydroxybutyrate) and poly(3-hydroxybutyrate-co-3-hydroxyvalerate) fiber mats, Int. J. Biol. Macromol. 40(3) (2007) 217-223.

[54] K. Sombatmankhong, N. Sanchavanakit, P. Pavasant, P. Supaphol, Bone scaffolds from electrospun fiber mats of poly(3-hydroxybutyrate), poly(3-hydroxybutyrate-co-3-hydroxyvalerate) and their blend, Polymer 48(5) (2007) 1419-1427.

[55] Y. Lee, N. Sridewi, S. Ramanathan, K. Sudesh, The influence of electrospinning parameters and drug loading on polyhydroxyalkanoate (PHA) nanofibers for drug delivery, Int. J. Biotech. Well. Indus. 4(4) (2015) 103-113.

[56] J.S. Choi, S.W. Lee, L. Jeong, S. Bae, B.C. Min, J.H. Youk, W.H. Park, Effect of organosoluble salts on the nanofibrous structure of electrospun poly(3-hydroxybutyrate-co-3-hydroxyvalerate), Int. J. Biol. Macromol. 34(4) (2004) 249-256.

[57] J. Ramier, M.B. Boubaker, M. Guerrouache, V. Langlois, D. Grande, E. Renard, Novel routes to epoxy functionalization of PHA-based electrospun scaffolds as ways to improve cell adhesion, J. Polym. Sci., Part A: Polym. Chem. 52(6) (2014) 816-824.

[58] M. Martínez Sanz, A. Lopez Rubio, M. Villano, C.S.S. Oliveira, M. Majone, M. Reis, J.M. Lagarón, Production of bacterial nanobiocomposites of polyhydroxyalkanoates derived from waste and bacterial nanocellulose by the electrospinning enabling melt compounding method, J. Appl. Polym. Sci. 133(2) (2016) 42486-42499.

[59] X. Jin, Y. Fan, Y. Xue, L. Wu, Y. Lu, J. Chen, X. Wang, D. Dong, F. Meng, Y. Lu, J.T. Wood, C. Tang, Electrospun CF-PHA nanocomposites: effect of surface modifications of carbon fibers, Int. J. Polym. Mater. Po 63(5) (2014) 262-267.

[60] M. Cheng, C. Lin, H. Su, P. Chen, Y. Sun, Processing and characterization of electrospun poly(3-hydroxybutyrate-co-3-hydroxyhexanoate) nanofibrous membranes, Polymer 49(2) (2008) 546-553.

[61] M. Zinn, B. Witholt, T. Egli, Occurrence, synthesis and medical application of bacterial polyhydroxyalkanoate, Adv. Drug Del. Rev. 53(1) (2001) 5-21.

[62] D. Grande, J. Ramier, D.L. Versace, E. Renard, V. Langlois, Design of functionalized biodegradable PHA-based electrospun scaffolds meant for tissue engineering applications, New. Biotechnol. (2016).

[63] J.S. Choi, S.W. Lee, L. Jeong, S.-H. Bae, B.C. Min, J.H. Youk, W.H. Park, Effect of organosoluble salts on the nanofibrous structure of electrospun poly(3-hydroxybutyrate-co-3-hydroxyvalerate), Int. J. Biol. Macromol. 34(4) (2004) 249-256.

[64] P. Lemechko, J. Ramier, D.L. Versace, J. Guezennec, C. Simon-Colin, P. Albanese, E. Renard, V. Langlois, Designing exopolysaccharide-graft-poly(3-hydroxyalkanoate) copolymers for electrospun scaffolds, React. Funct. Polym. 73(1) (2013) 237-243.

[65] H.-W. Tong, M. Wang, W.W. Lu, Electrospinning and Evaluation of PHBV-Based Tissue Engineering Scaffolds with Different Fibre Diameters, Surface Topography and Compositions, J. Biomater. Sci. Polym. Ed. 23(6) (2012) 779-806.

[66] H.-W. Tong, M. Wang, Electrospinning of Poly(Hydroxybutyrate-co-hydroxyvalerate) Fibrous Scaffolds for Tissue Engineering Applications: Effects of Electrospinning Parameters and Solution Properties, Journal of Macromolecular Science, Part B 50(8) (2011) 1535-1558.

[67] A. Ndreu, L. Nikkola, H. Ylikauppila, N. Ashammakhi, V. Hasirci, Electrospun biodegradable nanofibrous mats for tissue engineering, Nanomedicine 3(1) (2008) 45-60.

[68] K. Sombatmankhong, O. Suwantong, S. Waleetorncheepsawat, P. Supaphol, Electrospun fiber mats of poly(3-hydroxybutyrate), poly(3-hydroxybutyrate-co-3-hydroxyvalerate), and their blends, J. Polym. Sci., Part B: Polym. Phys. 44(19) (2006) 2923-2933.

[69] M.-L. Cheng, C.-C. Lin, H.-L. Su, P.-Y. Chen, Y.-M. Sun, Processing and characterization of electrospun poly(3-hydroxybutyrate-co-3-hydroxyhexanoate) nanofibrous membranes, Polymer 49(2) (2008) 546-553.

[70] T.H. Ying, D. Ishii, A. Mahara, S. Murakami, T. Yamaoka, K. Sudesh, R. Samian, M. Fujita, M. Maeda, T. Iwata, Scaffolds from electrospun polyhydroxyalkanoate copolymers: Fabrication, characterization, bioabsorption and tissue response, Biomaterials 29(10) (2008) 1307-1317.

[71] M. Ignatova, N. Manolova, I. Rashkov, N. Markova, Quaternized chitosan/κ-carrageenan/caffeic acid–coated poly(3-hydroxybutyrate) fibrous materials: Preparation, antibacterial and antioxidant activity, Int. J. Pharm. 513(1–2) (2016) 528-537.

[72] N. Tanadchangsaeng, D. Khanpimai, S. Kitmongkonpaisan, W. Chobchuenchom, T. Koobkokkruad, N. Sathirapongsasuti, Fabrication and characterization of electrospun nanofiber films of PHA/PBAT biopolymer blend containing chilli herbal extracts (capsicum frutescens L.), International Journal of Food Engineering 2(1) (2016).

[73] J.G. Fernandes, D.M. Correia, G. Botelho, J. Padrão, F. Dourado, C. Ribeiro, S. Lanceros Méndez, V. Sencadas, PHB-PEO electrospun fiber membranes containing chlorhexidine for drug delivery applications, Polym. Test. 34 (2014) 64-71.

[74] I. Han, K.J. Shim, J.Y. Kim, S.U. Im, Y.K. Sung, M. Kim, I.-K. Kang, J.C. Kim, Effect of poly(3-hydroxybutyrate-co-3-hydroxyvalerate) nanofiber matrices cocultured with hair follicular epithelial and dermal cells for biological wound dressing, Artif. Organs 31(11) (2007) 801-808.

[75] C. Lei, H. Zhu, J. Li, J. Li, X. Feng, J. Chen, Preparation and characterization of polyhydroxybutyrate-co-hydroxyvalerate/silk fibroin nanofibrous scaffolds for skin tissue engineering, Polymer Engineering & Science 55(4) (2015) 907-916.

[76] J. Yuan, J. Geng, Z. Xing, K. Shim, I. Han, J. Kim, I. Kang, J. Shen, Novel wound dressing based on nanofibrous PHBV–keratin mats, J. Tissue Eng. Regen. Med. 9(9) (2015) 1027-1035.

[77] E.I. Shishatskaya, E.D. Nikolaeva, O.N. Vinogradova, T.G. Volova, Experimental wound dressings of degradable PHA for skin defect repair, J. Mater. Sci. Mater. Med. 27(11) (2016) 165.

[78] J.-W.F.A. Simons, H. Adams, R.C. Cox, N. Dekker, F. Götz, A.J. Slotboom, H.M. Verheij, The Lipase from Staphylococcus aureus, Eur. J. Biochem. 242(3) (1996) 760-769.

[79] J.C. Santos, A.V. Paula, G.F.M. Nunes, H.F. de Castro, Pseudomonas fluorescens lipase immobilization on polysiloxane–polyvinyl alcohol composite chemically modified with epichlorohydrin, J. Mol. Catal. B: Enzym. 52-53 (2008) 49-57.

[80] W. Stuer, K.E. Jaeger, U.K. Winkler, Purification of extracellular lipase from Pseudomonas aeruginosa, J. Bacteriol. 168(3) (1986) 1070-1074.

[81] C. Hu, N. Xiong, Y. Zhang, S. Rayner, S. Chen, Functional characterization of lipase in the pathogenesis of Staphylococcus aureus, Biochem. Biophys. Res. Commun. 419(4) (2012) 617-620.

[82] K.M. Kamaly, K. Takayama, E.H. Marth, Acylglycerol Acylhydrolase (Lipase) Activities of Streptococcus lactis, Streptococcus cremoris, and Their Mutants, J. Dairy Sci. 73(2) (1990) 280-290.

[83] I.M. Khan, C.W. Dill, R.C. Chandan, K.M. Shahani, Production and properties of the extracellular lipase of Achromobacter lipolyticum, Biochimica et Biophysica Acta (BBA) - Enzymology 132(1) (1967) 68-77.

[84] A. Moraleda-Muñoz, L.J. Shimkets, Lipolytic Enzymes in Myxococcus xanthus, J. Bacteriol. 189(8) (2007) 3072-3080.

[85] J. Zhang, K. Kasuya, A. Takemura, A. Isogai, T. Iwata, Properties and enzymatic degradation of poly(acrylic acid) grafted polyhydroxyalkanoate films by plasma-initiated polymerization, Polym. Degradation Stab. 98(8) (2013) 1458-1464.

[86] K. Mukai, Y. Doi, Y. Sema, K. Tomita, Substrate specificities in hydrolysis of polyhydroxyalkanoates by microbial esterases, Biotechnol. Lett 15(6) (1993) 601-604.

[87] P.-S. Mok, D.H.-E. Ch'ng, S.-P. Ong, K. Numata, K. Sudesh, Characterization of the depolymerizing activity of commercial lipases and detection of lipase-like activities in animal organ extracts using poly(3-hydroxybutyrate-co-4-hydroxybutyrate) thin film, AMB Express 6(1) (2016) 97.

[88] P. Kanmani, K. Kumaresan, J. Aravind, S. Karthikeyan, R. Balan, Enzymatic degradation of polyhydroxyalkanoate using lipase from Bacillus subtilis, Int. J. Environ. Sci. Technol. (Tehran) 13(6) (2016) 1541-1552.

[89] S. Chanprateep, H. Shimizu, S. Shioya, Characterization and enzymatic degradation of microbial copolyester P(3HB-co-3HV)s produced by metabolic reaction model-based system, Polym. Degradation Stab. 91(12) (2006) 2941-2950.

[90] P. Azari, R. Yahya, C.S. Wong, S.N. Gan, Improved processability of electrospun poly[(R)-3-hydroxybutyric acid] through blending with medium-chain length poly(3-hydroxyalkanoates) produced by Pseudomonas putida from oleic acid, Mater. Res. Innov. 18(sup6) (2014) 345-349.

[91] L. Savenkova, Z. Gercberga, I. Bibers, M. Kalnin, Effect of 3-hydroxy valerate content on some physical and mechanical properties of polyhydroxyalkanoates produced by Azotobacter chroococcum, Process Biochem. 36(5) (2000) 445-450.

[92] S. Bruckner, S.V. Meille, L. Malpezzi, A. Cesaro, L. Navarini, R. Tombolini, The structure of poly(D-(-)-.beta.-hydroxybutyrate). A refinement based on the Rietveld method, Macromolecules 21(4) (1988) 967-972.

[93] M. Nerkar, Preparation and characterization of biopolymer compounds containing poly-3-hydroxyalkanoates and polylactic acid, Doctoral thesis, Queen's University, Kingston, Ontario, Canada (2014).

[94] S. Modi, K. Koelling, Y. Vodovotz, Assessment of PHB with varying hydroxyvalerate content for potential packaging applications, Eur. Polym. J. 47(2) (2011) 179-186.

[95] P.J. Barham, A. Keller, E.L. Otun, P.A. Holmes, Crystallization and morphology of a bacterial thermoplastic: poly-3-hydroxybutyrate, J. Mater. Sci. 19(9) (1984) 2781-2794.

[96] M.G. McKee, G.L. Wilkes, R.H. Colby, T.E. Long, Correlations of Solution Rheology with Electrospun Fiber Formation of Linear and Branched Polyesters, Macromolecules 37(5) (2004) 1760-1767.

[97] H. Sato, M. Nakamura, A. Padermshoke, H. Yamaguchi, H. Terauchi, S. Ekgasit, I. Noda, Y. Ozaki, Thermal behavior and molecular interaction of poly(3-hydroxybutyrate-co-3-

hydroxyhexanoate) studied by wide-angle X-ray diffraction, Macromolecules 37(10) (2004) 3763-3769.

[98] M. Martínez-Sanz, M. Villano, C. Oliveira, M.G.E. Albuquerque, M. Majone, M. Reis, A. Lopez-Rubio, J.M. Lagaron, Characterization of polyhydroxyalkanoates synthesized from microbial mixed cultures and of their nanobiocomposites with bacterial cellulose nanowhiskers, New. Biotechnol. 31(4) (2014) 364-376.

[99] L. Chen, M. Zhu, L. Song, H. Yu, Y. Zhang, Y. Chen, H.J. Adler, Crystallization behavior and thermal properties of blends of poly(3-hydroxybutyate-co-3-valerate) and poly(1,2-propandiolcarbonate), Macromol. Symp. 210(1) (2004) 241-250.

[100] E. Ten, J. Turtle, D. Bahr, L. Jiang, M. Wolcott, Thermal and mechanical properties of poly(3-hydroxybutyrate-co-3-hydroxyvalerate)/cellulose nanowhiskers composites, Polymer 51(12) (2010) 2652-2660.

[101] S. Rabiej, B. Ostrowska-Gumkowska, A. WŁOchowicz, Investigations of the crystallinity of PA-6/SPS blends by X-ray diffraction and DSC methods, Eur. Polym. J. 33(7) (1997) 1031-1039.

[102] O.W. Guirguis, M.T.H. Moselhey, Thermal and structural studies of poly (vinyl alcohol) and hydroxypropyl cellulose blends, Natural Science 4(1) (2012) 57-67.

[103] Y. Marois, Z. Ze, M. Vert, D. Xiaoyan, R. Lenz, R. Guidoin, Hydrolytic and enzymatic incubation of polyhydroxyoctanoate (PHO): A short-term in vitro study of a degradable bacterial polyester, J. Biomater. Sci. Polym. Ed. 10(4) (1999) 483-499.

[104] X. Wang, Z. Chen, X. Chen, J. Pan, K. Xu, Miscibility, crystallization kinetics, and mechanical properties of poly(3-hydroxybutyrate-co-3-hydroxyvalerate)(PHBV)/poly(3-hydroxybutyrate-co-4-hydroxybutyrate)(P3/4HB) blends, J. Appl. Polym. Sci. 117(2) (2010) 838-848.

[105] M. Sahebalzamani, E. Biazar, M. Shahrezaei, H. Hosseinkazemi, H. Rahiminavaie, Surface modification of PHBV nanofibrous mat by laminin protein and its cellular study, Int. J. Polym. Mater. Po 64(3) (2015) 149-154.

[106] S. Kiselioviene, O. Baniukaitiene, V. Harkavenko, N.A. Babenko, J. Liesiene, Cellulose Hydrogel Sheets for Wound Dressings, Cellul. Chem. Technol. 50(9-10) (2016) 915-923.

[107] M.C. Straccia, I. Romano, A. Oliva, G. Santagata, P. Laurienzo, Crosslinker effects on functional properties of alginate/N-succinylchitosan based hydrogels, Carbohydr. Polym. 108(Supplement C) (2014) 321-330.

[108] S.M. Lee, I.K. Park, Y.S. Kim, H.J. Kim, H. Moon, S. Mueller, Y.-I. Jeong, Physical, morphological, and wound healing properties of a polyurethane foam-film dressing, Biomater. Res. 20(1) (2016) 15.

[109] N. Fetisova, V. Tsetlin, Main group of parameters for evaluating film-forming properties in aerosol packages for the treatment of an operation field and for the sealing of wounds, Pharm. Chem. J. 10(8) (1976) 1071-1075.

[110] Z.-M. Huang, C.-L. He, A. Yang, Y. Zhang, X.-J. Han, J. Yin, Q. Wu, Encapsulating drugs in biodegradable ultrafine fibers through co-axial electrospinning, Journal of Biomedical Materials Research Part A 77A(1) (2006) 169-179.

[111] N. Naveen, R. Kumar, S. Balaji, T.S. Uma, T.S. Natrajan, P.K. Sehgal, Synthesis of Nonwoven Nanofibers by Electrospinning – A Promising Biomaterial for Tissue Engineering and Drug Delivery, Adv. Eng. Mater. 12(8) (2010) B380-B387.

[112] W. Ji, F. Yang, J.J.J.P. van den Beucken, Z. Bian, M. Fan, Z. Chen, J.A. Jansen, Fibrous scaffolds loaded with protein prepared by blend or coaxial electrospinning, Acta Biomater. 6(11) (2010) 4199-4207.

[113] K.-C. Hoang, M. Tseng, W.-J. Shu, Degradation of polyethylene succinate (PES) by a new thermophilic Microbispora strain, Biodegradation 18(3) (2007) 333-342.

[114] Y. Tokiwa, T. Suzuki, K. Takeda, Two Types of Lipases in Hydrolysis of Polyester, Agric. Biol. Chem. 52(8) (1988) 1937-1943.

[115] A.J. McBain, R.G. Ledder, L.E. Moore, C.E. Catrenich, P. Gilbert, Effects of quaternary-ammonium-based formulations on bacterial community dynamics and antimicrobial susceptibility, Appl. Environ. Microbiol. 70(6) (2004) 3449-3456.

[116] T.P. L., H.A. N., S. Anselm, S. Gregory, L. Bernd, M. Dilip, R.T. W., A study on the ability of quaternary ammonium groups attached to a polyurethane foam wound dressing to inhibit bacterial attachment and biofilm formation, Wound Repair Regen. 23(1) (2015) 74-81.

[117] R. Sedghi, A. Shaabani, Electrospun biocompatible core/shell polymer-free core structure nanofibers with superior antimicrobial potency against multi drug resistance organisms, Polymer 101(Supplement C) (2016) 151-157.

[118] R. Talon, M.C. Montel, Hydrolysis of esters by staphylococci, Int. J. Food Microbiol. 36(2) (1997) 207-214.